AD-A189 151 MODE PRIMING IN AN OVERMODED GYROTRON OSCILLATOR(U) 1/1
NAVAL RESEARCH LAB WASHINGTON DC A H MCCURDY ET AL.
19 OCT 87 NRL-MR-6102

UNCLASSIFIED F/G 20/3 NL

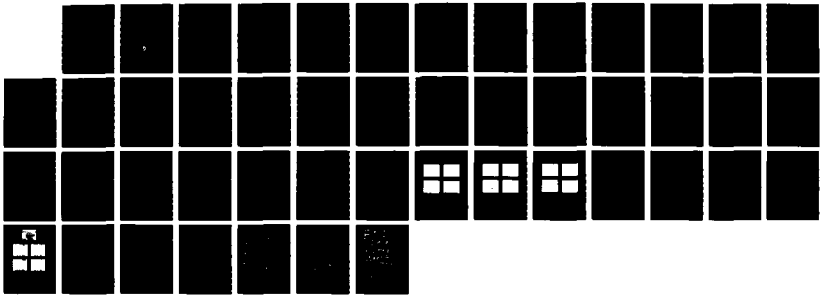

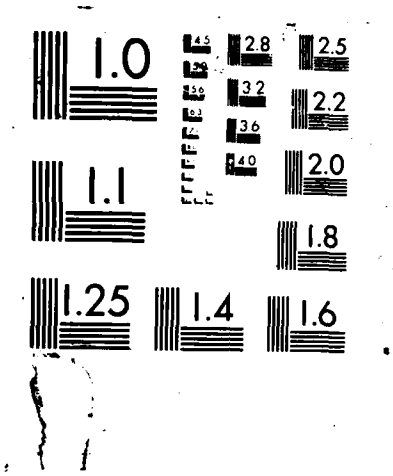
1.0
1.1
1.25
1.4
1.6
1.8
2.0
2.2
2.5
2.8
3.2
3.6
4.0

Naval Research Laboratory

Washington, DC 20375-5000

NRL Memorandum Report 6102

Mode Priming in an Overmoded Gyrotron Oscillator

ALAN H. MCCURDY

Microwave and Millimeter Wave Tube Technology Branch
Electronics Technology Division

CARTER M. ARMSTRONG

Applied Physics Section
Yale University
New Haven, CT 06520

October 19, 1987

Approved for public release; distribution unlimited.

SECURITY CLASSIFICATION OF THIS PAGE

REPORT DOCUMENTATION PAGE

1a. REPORT SECURITY CLASSIFICATION UNCLASSIFIED	1b. RESTRICTIVE MARKINGS
2a. SECURITY CLASSIFICATION AUTHORITY	3. DISTRIBUTION/AVAILABILITY OF REPORT Approved for public release; distribution unlimited.
2b. DECLASSIFICATION/DOWNGRADING SCHEDULE	
4. PERFORMING ORGANIZATION REPORT NUMBER(S) NRL Memorandum Report 6102	5. MONITORING ORGANIZATION REPORT NUMBER(S)
6a. NAME OF PERFORMING ORGANIZATION Naval Research Laboratory 6b. OFFICE SYMBOL (*If applicable*) Code 6842	7a. NAME OF MONITORING ORGANIZATION
6c. ADDRESS (*City, State, and ZIP Code*) Washington, DC 20375-5000	7b. ADDRESS (*City, State, and ZIP Code*)
8a. NAME OF FUNDING/SPONSORING ORGANIZATION Office of Naval Technology 8b. OFFICE SYMBOL (*If applicable*) ONT	9. PROCUREMENT INSTRUMENT IDENTIFICATION NUMBER
8c. ADDRESS (*City, State, and ZIP Code*) Arlington, VA 22217	10. SOURCE OF FUNDING NUMBERS PROGRAM ELEMENT NO. 62762N; PROJECT NO.; TASK NO XF62-584-100; WORK UNIT ACCESSION NO. DN480-973

11. TITLE (*Include Security Classification*)
Mode Priming in an Overmoded Gyrotron Oscillator

12. PERSONAL AUTHOR(S) McCurdy,* A.H. and Armstrong, C.M.

13a. TYPE OF REPORT	13b. TIME COVERED	14. DATE OF REPORT (*Year, Month, Day*)	15. PAGE COUNT
Memorandum	FROM _____ TO _____	19 October 1987	47

16. SUPPLEMENTARY NOTATION
*Applied Physics Section, Yale University, New Haven, CT 06520

17. COSATI CODES			18. SUBJECT TERMS (*Continue on reverse if necessary and identify by block number*)
FIELD	GROUP	SUB-GROUP	Gyrotron Overmoded Microwave Oscillator

19. ABSTRACT (*Continue on reverse if necessary and identify by block number*)

Axial mode control in a gyrotron oscillator is accomplished by injection of an external signal into the oscillator. The mechanism by which the selection technique works is that of priming, where the injected signal is required only during the early stages of oscillation growth. Like phase priming, mode control can be obtained with an external signal power level nearly 40 dB below the oscillator power level and with an external frequency closer to the operating mode than any other. It is found that the external signal can select a mode when the free gyrotron operation skips between modes from pulse to pulse. Also, in certain conditions, a single stable mode can be changed to a different mode by a priming signal. Finally a case is studied where a bistable system (two simultaneous modes) is reduced to a single mode because of the external signal. Mode control is used as a diagnostic to investigate the coupling of an external electromagnetic wave to the electron beam via electron cyclotron resonance absorption. Beam-wave coupling is studied as a function of the polarization of the input drive signal. It is found that the external electromagnetic signal couples best when launched as a right-hand circularly polarized wave. The theoretical ratio (55.2) of the coupling factors for the right- and left-hand electromagnetic waves is found to be consistent with the experimentally value within the uncertainties of the measurement.

20. DISTRIBUTION/AVAILABILITY OF ABSTRACT ☐ UNCLASSIFIED/UNLIMITED ☐ SAME AS RPT ☐ DTIC USERS	21. ABSTRACT SECURITY CLASSIFICATION
22a. NAME OF RESPONSIBLE INDIVIDUAL C.M. Armstrong	22b. TELEPHONE (*Include Area Code*) (202) 767-0032 22c. OFFICE SYMBOL Code 6842

DD FORM 1473, 84 MAR 83 APR edition may be used until exhausted
All other editions are obsolete

SECURITY CLASSIFICATION OF THIS PAGE

*U.S. Government Printing Office: 1985—507-047

CONTENTS

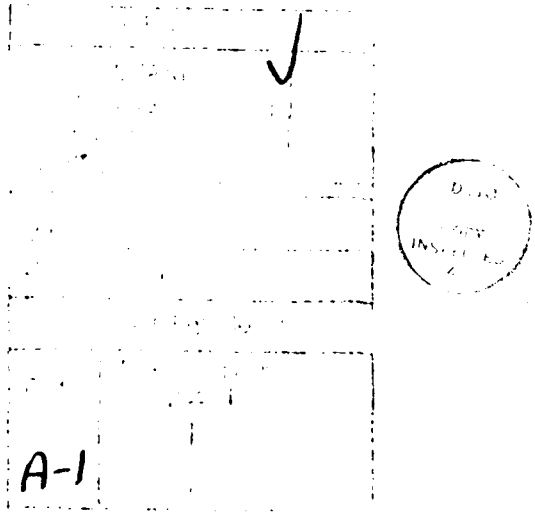

MODE PRIMING IN AN OVERMODED GYROTRON OSCILLATOR

I. Introduction

As gyrotron oscillators are designed to operate at megawatt power levels and frequencies over 100 GHz the problem of mode competition becomes severe.[1,2] The higher power levels force the characteristic dimension d of the gyrotron cavity to be made large compared to the operating wavelength. The relative frequency separation between modes in the oscillator scales as $(\lambda/d)^2$, where λ is the radiation wavelength. Thus the frequency separation between modes becomes small as the gyrotron operating frequency is increased. The problems caused by parasitic modes can include decrease in electronic efficiency, uneven thermal wall loading[3] and multiple output frequencies.

Several methods have been proposed to remedy this problem in the gyrotron. These fall generally into the catagories of modifying the beam or cavity geometry or tailoring the gyrotron startup conditions. The method used here falls into the second catagory.

One beam geometry modification involves placing the electron beam at a position in the cavity where the transverse electric field of the desired mode is strong but those of competing modes are weak.[4] Another, superior method, is to premodulate the electron beam at the desired frequency of operation to enhance the interaction with a given mode.[5,6] This technique is similar to the prebunching concept used for phase control of gyrotrons.[7,8] Systems to modify cavity geometry to

Manuscript approved August 11, 1987.

control unwanted modes include slotted wall resonators,[9-10] resonators with lossy inserts,[11] coaxial resonators,[12,13] and the quite successful complex cavities.[13,14]

Mode control via tailoring of the gyrotron startup conditions is advantageous in that it provides a more flexible means of achieving the desired output mode. Careful control of the electron beam perpendicular and parallel velocities has provided mode selectivity due to the dependence of mode start oscillation currents on these beam parameters.[15]

The method used here entails injection of a small external signal into the oscillator during the early stages of oscillation buildup. The effect of the signal is to slightly modulate the electron beam, by electron cyclotron resonance absorption, at the frequency of the desired mode. This mode is then given an advantage in the ensuing competition with other growing modes. This same mechanism should be enhanced by injecting the signal into a prebunching cavity as mentioned above.

II. Experimental

The experimental configuration is shown in Fig. 1(a). The gyrotron cavity is a cylindrical waveguide, approximately six free space wavelengths in length (40 cm), terminated by discontinuities at the gun and collector ends. The cavity radius is 1.75 cm. The beam parameters are 25 KeV at 2 A with a perpendicular-to-parallel velocity ratio (α) of about one. The output radiation is near 5 GHz in 2.5 μs pulses at a 60 Hz repetition rate. Power is coupled out of the gyrotron via four symmetrically placed capacitively-coupled probes at the cavity midplane (Fig. 1(b)). The probes are flush with the tube wall and weakly couple matched loads in the output lines to the cavity, (coupling factors of about .1). Because of the closed tube ends and the weakly coupled probes the loaded quality factors of the lowest four axial modes are all about 1200.

A schematic of the experimental setup is shown in Fig. 2(a). The external signal is generated from a stable (3 KHz pulse-to-pulse jitter) sweep oscillator, amplified, and then injected via a circulator through one of the probes. Adequate isolation (40 dB) is used to prevent any of the gyrotron output power from feeding back into the external source. The gyrotron output rf is monitored through another probe. The other two probes are terminated by matched loads. The modes of gyrotron oscillation are determined from frequency and amplitude characteristics after passing the output through a tuneable bandpass filter (3 MHz bandpass, cavity type).

The relative phase between the output radiation and the external drive is measured by a mixer phase diagnostic.[16] DC blocks are used in the input and output probe lines to prevent any currents generated by beam interception at the probes from passing through the external apparatus. Other experiments are carried out by exciting two probes by an external signal. Fig 2(b) shows the experimental schematic for these investigations. The distinguishing features are the phase shifter in one input line and attenuators to balance the drive signal to the two probes.

The characteristics of the gyrotron as calculated from linear theory[17] are shown in Fig. 3. The start oscillation currents for the first three TE_{11n} modes are shown in Fig. 3(a) as a function of axial magnetostatic field. As expected, there are n regions of excitation of each mode. Though the theory does not take into account mode competition effects, it is clear from the similar (~.1 A) start oscillation currents and the large overlap of regimes of excitation of the different modes that there will be significant mode competition. The spacing between axial electromagnetic modes in the cold gyrotron cavity is approximately:

$$\Delta\omega_m = \left(\frac{c\,\pi}{L}\right)^2 \frac{n_1^2 - n_2^2}{2\,\omega}$$

where L is the cavity length, c is the speed of light, ω the mode frequency and n_1 and n_2 the axial mode numbers. When this spacing is on the order of the linewidth of

the gyrotron oscillation then mode competition is likely. The gyrotron linewidth is given by the transit time broadening:

$$\Delta\omega_b = \frac{\pi v_o}{L}$$

where v_o is the beam axial velocity. In our experiment $\frac{\Delta\omega_m}{2\pi} \cong 42$ MHz between the TE_{111} and TE_{112} modes and 70 MHz between the TE_{113} and TE_{112} modes, (L=40 cm). The line broadening is about 78 MHz using an α of 1.0 and a beam voltage of 25 KeV. Mode competition is expected since the gyrotron gain bandwidth is of the same order as the spacing between the lower order modes.

Fig. 3(b) gives the predicted oscillation frequencies of the lowest order axial modes. In the figure the frequencies are normalized to the cold cavity frequency of the TE_{111} mode. The modal separations are close to that predicted previously and amount to about 1 % of the operating frequency.

III. Theory

Work on the simple quasi-linear theory of multi-mode electromagnetic oscillations started with Lamb's study of lasers.[18] This theory was later applied to the gyrotron oscillator.[19,20] The method involves the assumption that the growth rates are slow compared to the electron transit time. The time dependent equations for the electric field are averaged over an rf period thus yielding rate equations for the amplitudes of the modes. The electron susceptibility (or polarizability) is expanded in powers of the mode amplitudes. This expansion is terminated after retaining a few nonlinear terms by assuming that the mode amplitudes are small. For two modes the real part of the electron susceptibility has the form:

$$\chi_i \sim \alpha_i - \beta_i A_i^2 - \Theta_{ij} A_j^2$$

where A_i is the amplitude of the i^{th} mode, α_i is the linear growth rate, β_i is the self-saturation coefficient, and Θ_{ij} is the cross-saturation coefficient of the other oscillating mode. In the actual distributed nature of the gyrotron these coefficients are integrals depending on particle trajectories and spacial dimensions.[21] The rate equations are simply:

$$\frac{d(A_i^2)}{dt} - (\alpha_i - \beta_i A_i^2 - \Theta_{ij} A_j^2) A_i^2 = 0 \qquad (1)$$

The equilibrium points occur when the amplitude growth is zero. The growth is zero when the following relationships are satisfied:

$$\alpha_1 - \beta_1 A_1^2 - \Theta_{12} A_2^2 = 0 \quad \text{or} \quad A_1 = 0$$
$$\text{and} \qquad \alpha_2 - \beta_2 A_2^2 - \Theta_{21} A_1^2 = 0 \quad \text{or} \quad A_2 = 0 \; . \qquad (2)$$

Lamb showed that the type of behavior of the system described by equation (1) exhibits can be reduced to three cases depending on the relative sizes of the coefficients. The two modes are either weakly coupled, critically coupled, or strongly coupled.

Weakly coupled modes can result in either of two different steady states. If the linear growth of one of the modes is much larger than the other, then the faster growing mode may tend to quench the slower through the coefficient Θ_{ij}. If the growth rates are similar then a steady state can exist in which both modes oscillate independently (bistable steady state). The requirement for weak coupling is that $\beta_1\beta_2 > \Theta_{12}\Theta_{21}$ (it is assumed that $\beta_i > 0$). Thus the self-saturation effects are larger than the cross-saturation ones. When the relation $\beta_1\beta_2 < \Theta_{12}\Theta_{21}$ is satisfied the two modes are strongly coupled. A rough diagram of the solutions to the rate equations in this case is shown in Fig. 4, (for $\alpha_1=\alpha_2$, $\beta_1=\beta_2$, and $\Theta_{12}=\Theta_{21}$). There are two stable

equilibrium points at (A_1=0, A_2=A_y and (A_1=A_x, A_2=0), where A_x and A_y are solutions to the quadratic expressions in equation (2). In either case only one mode oscillates in the steady state. The curves in Fig. 4 show the trajectories the system follows as steady state is approached. The origin of the oscillation is noise which contains both of the frequencies of modes 1 and 2 plus whatever surrounding frequencies the finite quality factor of the oscillator will support. This initial noise level determines on which trajectory in Fig. 4 the oscillation will progress. Since the noise is random in character it is possible, in a pulsed oscillator, that different modes will be present from pulse to pulse.

If a small external signal is injected into the oscillator the choice of trajectory in Fig. 4 is affected. The drive is assumed to be small enough so as to be of consequence to the dynamics of the system only during the early stages of oscillation buildup. A qualitative understanding of the effect of the drive can be gained by considering the signal and noise to together produce a new initial condition. If the drive signal is at the frequency of mode 1, (and signal amplitude >> noise), then the system will initially have a much larger amplitude of mode 1 than mode 2 and will hence follow one of the trajectories below the 45° line. These all lead to stable mode 1 oscillation in the steady state. The same type of effect could be generated for mode 2 by injection of a signal at that frequency. Thus the mode selectivity of the external signal is demonstrated.

IV. Results and Discussion

Mode Control

The experimental map of the different regimes of pure mode excitation of the free-running gyrotron is shown in Fig. 5. At the lower beam currents the lowest order mode usually predominates. It is found that throughout the range of gyrotron

operating parameters studied, (with an approximately flat magnetic field profile), the gyrotron oscillates in a single mode in the steady state. In the regions of Fig. 5 between those for pure mode excitation the gyrotron skips between modes from pulse to pulse.

The mode selection phenomenon is shown by the oscillographs in Fig. 6. Fig. 6(a) shows a crystal dioide trace of the free-running gyrotron rf output. Here the output is skipping between the TE_{111} and TE_{112} modes from pulse to pulse. The magnetic field is 1.87 kG and the beam current is .77 A. The presence of two modes can usually be determined from the fluctuations in amplitude of the rf output signal. Figure 6(b) shows the effect of an external driving signal at 5.141 GHz, the frequency of the TE_{112} mode. The gyrotron output is stabilized in the desired mode. Likewise applying a driving signal at the frequency of the TE_{111} mode (5.093 GHz) can stabilize the gyrotron in that mode, (Fig. 6(c)). The drive power is about .7 W in both cases. The coupling factor of the driven probe (#4) is .052 so only about 20 % of the drive power is actually coupled into the gyrotron.

The photograph in Fig 6(d) shows the relative phase between the drive signal and the gyrotron oscillation as measured by the mixer phase diagnostic. The relative phase is stable from pulse to pulse only at the leading edge of the oscillation. As the oscillation progresses, there is phase slippage because the gyrotron frequency varies from the drive frequency from pulse to pulse. This shows that the effect of the drive signal is confined to times during the gyrotron oscillation buildup. This is reasonable since the external signal power level inside the cavity is orders of magnitude smaller than that of the steady-state oscillation.

Fig. 7 shows a more careful study of the temporal dependence of the mode control phenomenon. Here a pulsed drive signal of approximately 50 ns duration is used. All photographs in Fig. 7 display signals from the crystal diodes monitoring the gyrotron output power (lower trace) and the drive signal power (top trace).

Fig. 7(a) shows the free oscillation skipping between the TE_{111} and TE_{113} modes (predominantly in TE_{113}). When a drive pulse, at the frequency of the TE_{111} mode, is applied early in the oscillation buildup, Fig. 7(b), there is a slight enhancement of the fraction of gyrotron pulses which are in the TE_{111} mode. The drive signal is injected about 350 ns before the oscillation saturation. Moving the drive pulse about 50 ns later in the buildup has a striking effect. The gyrotron output now consists solely of the TE_{111} mode. Figure 7(d) shows the effect of a drive signal applied ~ 200 ns before oscillation saturation. Once again, the drive only slightly affects the gyrotron performance. The phenomena displayed in the phase control measurement of Fig. 6(d) and the temporal dependence of oscillator control in Fig. 7 is that of priming.[22,23] Priming typically involves only control of the startup phase of a pulsed oscillator. Here we see mode control by a similar mechanism. Hence the effect is termed "mode priming". Mode control by injection of an external signal has been demonstrated in TEA-CO_2 lasers.[24] Their method, sometimes referred to as "injection seeding", has not been connected with the previous, more general, work on oscillator priming[25] to which it is obviously related.

In a primed system the small external signal only has an effect on the oscillation for a short period of time in the early stages of oscillation buildup. The oscillator steady state frequency is not affected by the injected signal though the relative phase relationship of the oscillator to the drive is not completely random. The oscillator starts each pulse very nearly in phase with the drive signal. Finally it is seen that the priming signal may select, by frequency difference, among several possible modes.

A single steady mode can be switched to another stable nearby mode by a priming signal of the appropriate frequency. Fig. 8 shows an example of this degree of control. The experimental parameters in this case are a magnetic field of 1.902 kG and a beam current of 1.35 A. The free steady state oscillation is in the TE_{113} mode as

can be seen from Fig. 5. The photograph in Fig. 8(a) shows the crystal diode signal with the bandpass filter located at 5.251 GHz. A pure TE_{113} mode is present and no mode skipping is apparent. Tuning the filter to 5.186 GHz (the expected frequency of the TE_{112} mode) reveals that there is no TE_{112} mode present in the free-running case, Fig 8(b). When a drive signal of 1.1 W (200 mW into the cavity) is introduced at 5.186 GHz the oscillation switches from the TE_{113} mode (Fig. 8(c)) to the TE_{112} mode (Fig. 8(d)). The consequences of this result are as follows. Even though the start oscillation threshold of several modes have been exceeded in the experiment of Fig. 8 only one mode survives in the steady state. In practice, this mode may not be the desired one. It is not even always possible to reach the regime of highest efficiency of the desired mode without encountering mode competition effects.[26] This regime may be in the "hard excitation" region which is below the start oscillation current of the given mode.[27] The external mode priming signal can expand the range over which a given mode can maintain stable operation. Thus the previously inaccessible regimes can support stable operation in the desired mode. In addition, the priming signal can provide access to the hard excitation regime.[22]

The increase in scope of stable TE_{111} operation due to a 20 W drive signal is shown on the plane of beam current vs. magnetic field, (I-B plane), in Fig. 9. The regime of stable TE_{111} oscillation in the undriven case is shown for comparison. The drive frequency is adjusted to equal what the TE_{111} mode would be expected to have at the particular gyrotron operating parameters were there no other modes present. The area in the I-B plane in which a stable TE_{111} mode can be maintained increases by about 50 % due to the applied drive signal. It is particularly easy to prime a given mode if it is a strong oscillation and the competing modes are weak. Note that the driven TE_{111} oscillation penetrates both the regions of pure free TE_{112} and TE_{113} operation. The most significant success, however, is penetration of regions where mode skipping occurs in the undriven case (compare Figs. 9 and 5). A strong

stubborn TE_{112} backward oscillation can not be overcome (slightly above 2.0 kG on the figures).

Fig. 10 shows the increased region of pure TE_{112} mode oscillation due to the external signal. The driven TE_{112} mode does not easily displace the region of pure TE_{111} oscillation since the TE_{111} is strong in this portion of the I-B plane. However there is good success in overcoming regions of pure TE_{113} and in mode skipping regions. The forward TE_{112} melds into the backward component at ~1.925 kG. Fig. 11 shows the same experiment on the TE_{113} mode. In this case stable operation is achieved in areas that were pure TE_{111} in the free case. The TE_{111} oscillation weakens at higher beam currents. The conclusion from these experiments is that the regime of pure oscillation of any mode can be significantly enhanced by the application of an external signal tuned to the correct frequency. A greater portion of the gyrotron operating parameter space is then available.

Fig. 12 shows the minimum drive power required to achieve pure mode operation as a function of drive frequency. Here pure mode operation is defined to mean that greater than 99.95% of all gyrotron output pulses are in the desired mode. A magnetic field near 1.84 kG and a .55 A beam current yield a steady TE_{112} mode oscillation. The drive signal primes the TE_{111} mode. The general shape of the curve in Fig. 12 is an inverted gaussian with slightly different behavior for higher drive frequencies (f_{drive}-$f_{oscillation}$ > 10 MHz) than lower (f_{drive}-$f_{oscillation}$ < 10 MHz). A cavity resonance profile is included for comparison. It is clear that the change in mode control with drive frequency is not simply due to the finite resonance width of the cavity. As intuitively expected, generally the further the drive frequency is from the TE_{111} frequency the more drive power required for pure mode operation. Perhaps the most striking feature of Fig. 12 is that the drive frequency at which the least drive power is required for pure mode oscillation is not the same as the TE_{111} oscillation frequency. In this experiment and in all others investigated, (including

an experiment at the second harmonic of the cyclotron frequency), better control is wielded by a drive signal of frequency slightly above the oscillation frequency. This same feature is present whether the competing mode frequency is above or below that of the driven mode. The explanation may be that for such a long gyrotron cavity there are several cyclotron resonance absorption bands above the frequency for which emission occurs, (assuming the field frequency is near the cyclotron frequency). This does not explain why there is no control at lower frequencies since the beam loading once again becomes positive.

For drive frequencies near that of the desired oscillation the power required for operation in the TE_{111} mode is close to 25 dB below the TE_{111} oscillation power (power is measured outside of the cavity). When the cavity coupling factor of .052 is taken into account the drive-to-oscillator power ratio required for mode control, (compared inside the cavity), is -37 dB at the optimal drive frequency. In addition, the bandwidth over which control can be maintained is a large fraction of the intermode frequency separation.

An experiment with two simultaneously oscillating modes is also carried out. In this case the two modes are weakly coupled so that the resulting configuration can be bistable. The modes are decoupled by broadening the gain bandwidth of the gyrotron via a tapered magnetic field profile along the tube axis. Thus the two modes can oscillate almost indepedently using different parts of the gain medium. Fig. 13 shows photographs detailing the effect of a drive signal on this system. The output of the free-running gyrotron is shown in Fig 13(a). TE_{111} and TE_{112} modes beat against each other thereby amplitude modulating the output at about 50 MHz. The bandpass filter locates the TE_{112} mode at 5.156 GHz (Fig. 13(b)) and the TE_{111} at about 5.099 GHz (Fig. 13(c)). It can be seen from these two figures that the TE_{112} starts first and has a more rapid growth rate than the TE_{111}. The magnetic field is linearly tapered with the lowest value near the electron gun. Thus the TE_{111} mode is

resonant with the electron beam near the gun. Since the beam is unmodulated at this point it is understandable that the TE_{111} mode can continue to grow after the TE_{112} mode has saturated. If the TE_{112} was not the faster growing mode one would not expect it to ever appear since the beam modulation due to the TE_{111} would provide cross-saturation. Thus the beam is essentially prebunched by the mode resonant with the beam near the gun. Fig. 13(d) and (e) show the effect of applying a signal at the frequency of the TE_{111} mode. The oscillation in the TE_{112} mode ceases (13(d)) and that of the TE_{111} is enhanced (13(e)). The reason for this effect is that with the boost of the drive signal the TE_{111} mode reaches the nonlinear regime first, as if it were the faster growing mode. When the TE_{112} is driven it is found that there is virtually no effect. Since the TE_{112} mode starts first in the free-running case and cannot quench the TE_{111} there is no reason to assume things should be any different in the driven case. Reversing the direction of the magnetic field taper caused a single mode oscillation in the TE_{112} mode. This is because the fastest starting mode is once again upstream of the slower. There will be no mode competition in this case.

An experiment at the second harmonic of the cyclotron frequency shows the same phenomena. Operating the gyroton at magnetic fields near 1.6 kG at beam currents above 1.0 A and a voltage of 22 kV generates radiation in the range 8.4 to 8.7 GHz. The cavity modes in this case are the TE_{21n} family. Fig. 14 shows the minimum drive power required for pure mode operation in the TE_{214} mode as a function of drive frequency. The free-running behavior in this case is mode skipping between the TE_{214} and TE_{215}. Though only the top portion of the curve is shown it is clear that the required drive power levels are similar to the previous experiments and the point of maximum control occurs at a drive frequency slightly above that of the free TE_{214} oscillation. Thus the same mode control phenomena observed previously at the fundamental cyclotron frequency scales to the higher harmonics.

Coupling Between Beam and E-M Wave

Using the fact that the degree of coupling of an rf signal to the electron beam can be determined by the degree of mode control observed, an investigation is made into the nature of the electromagnetic wave which participates in the electron cyclotron maser instability. The theory has shown that the predominant electromagnetic forces on the electrons are due to the right-hand circularly polarized (RHCP) transverse electric wave.[28-30] It has been found that the equation for the perturbation in electron position by a transverse electromagnetic wave contains terms proportional to $(\pm\omega - k_z v_z - n\Omega)^{-2}$. The largest deviations in electron position are produced by these terms when $\pm\omega - k_z v_z - n\Omega \cong 0$. Obviously the plus sign in front of ω must be chosen for this synchronism criterion to be satisfied. This means that the electromagnetic wave rotates in the same direction as the beam cyclotron wave. The electrons thus feel virtually static fields in the co-rotating frame of reference. The experimental objective is to show that regardless of how the electromagnetic wave is polarized, upon injection into the gyrotron, it is only the RHCP component of the wave which will couple to the electron beam.

Injecting a signal (at the cyclotron fundamental frequency) into the gyrotron through a single probe exites a standing TE_{11} wave. The structure of this field in the cylindrical gyrotron cavity is given by:

$$\mathbf{E} = E\left(\frac{1}{k_\perp r} J_1(k_\perp r)\sin\phi\,\hat{r} + \frac{dJ_1(k_\perp r)}{dk_\perp r}\cos\phi\,\hat{\phi}\right)e^{j\omega t} \qquad (3)$$

Here the dependence on axial coordinate is suppressed for compactness of presentation. The polar coordinates are r and ϕ and the probe is located at $\phi=90^\circ$, (see Fig. 15(a)). Using the abbreviations:

$$A = \frac{1}{k_\perp r} J_1(k_\perp r) \quad \text{and} \quad B = \frac{dJ_1(k_\perp r)}{dk_\perp r} \quad ,$$

the linearly polarized wave in (3) can be written in terms of circularly polarized waves: [31]

$$E = A\left(-\frac{E}{2} e^{j(\omega t+\phi+\pi/2)} + \frac{E}{2} e^{j(\omega t-\phi+\pi/2)}\right)\hat{r} + B\left(\frac{E}{2} e^{j(\omega t+\phi)} + \frac{E}{2} e^{j(\omega t-\phi)}\right)\hat{\phi} \qquad (4)$$

Here the right-hand (left-hand) component has a negative (positive) sign in the exponential. The time averaged power in the wave:

$$\langle P \rangle = \frac{1}{2} \int_S \mathrm{Re}\{E \times H^*\} \cdot dS$$

where integration is taken over the cavity cross-section s, yields a power into the right-hand component, (using the orthogonality of RHCP and LHCP waves), of:

$$\langle P_{RH} \rangle = \frac{E^2}{8} \frac{k_z}{\omega \mu_o} \int_S (A^2 + B^2) r \, d\phi \, dr = \frac{P_{IN}}{2} \qquad (5)$$

It can easily be shown that the power into the left-hand component is identical to that of equation (5). Thus half of the probe input power, P_{IN}, goes to the right-hand wave as is expected since the total wave is linearly polarized.

The configuration of the two probe excitation is shown in Fig. 15(b). The probes are spacially separated by 90^o in azimuthal coordinate and are excited with amplitudes E_1 and E_2 and with a phase difference Θ. The total drive power into the

gyrotron is $P_1 + P_2 = P_{IN}$. The total field in the input wave is the sum of equation (3), (with $E=E_1$), and

$$\mathbf{E}_2 = E_2 \left(A \cos\phi \, \hat{r} - B \sin\phi \, \hat{\phi} \right) e^{j(\omega t + \Theta)} \quad , \tag{6}$$

the field excited by the second probe. Writing equation (6) in terms of circularly polarized waves and adding to equation (4):

$$\mathbf{E}_{TOTAL} = \frac{A}{2}\left(e^{j(\omega t+\phi)}\left[E_2 e^{j\Theta} - E_1 e^{j\pi/2} \right] + e^{j(\omega t-\phi)}\left[E_2 e^{j\Theta} + E_1 e^{j\pi/2} \right] \right) \hat{r}$$

$$+ \frac{B}{2}\left(e^{j(\omega t+\phi)}\left[E_2 e^{j(\Theta+\pi/2)} + E_1 \right] + e^{j(\omega t-\phi)}\left[E_1 - E_2 e^{j(\Theta+\pi/2)} \right] \right) \hat{\phi}$$

Finding the time averaged power into the right- and left-hand waves as before:

$$\langle P \rangle = \frac{1}{2}\frac{k_z}{\omega\mu_o}\left[E_1^2 + E_2^2 \pm 2 E_1 E_2 \sin\Theta \right] \int_S (A^2 + B^2) r \, d\phi \, dr \tag{7}$$

where the upper (lower) sign is taken for the power into the right- (left-) hand circularly polarized wave. For the special case of E_2 leading E_1 by 90^o ($\Theta=90^o$) the power into the right hand wave in equation (7) is:

$$\langle P_{RH} \rangle = \frac{1}{2} P_{IN} + \sqrt{P_1 P_2} \quad . \tag{8}$$

Further specializing to equal amplitudes injected into the two probes:

$$\langle P_{RH} \rangle = P_{IN} \tag{9}$$

and all of the input power couples to the RHCP electromagnetic wave. Intuitively this makes sense because the linearly polarized waves excited by each probe can be decomposed into oppositely travelling circular waves. For equal amplitudes the 90^{o} temporal phase lead adds to the 90^{o} spacial separation to cause the right hand components of the two probes to add constructively while the left hand components cancel. As long as the probe diameter is a small fraction of the cavity circumference a pure circularly or linearly polarized wave may be excited. In the experiment, cold test results indicate that the assumption that a single probe excites a pure linearly polarized wave is justified. More than 80 % of the input power was injected into the linearly polarized component.

The degree of control of the modes in the gyrotron is measured statistically by averaging the signal from a crystal diode monitoring gyrotron output power. The gyrotron is tuned to a parameter region where a single stable mode oscillates in the free-running case. The input drive signal has a frequency equal to that of a competing mode. As the drive power couples to the electron beam the gyrotron begins to mode skip into the driven mode. The input power level is adjusted so that even when the drive power couples optimally to the beam the gyrotron continues to mode skip to some degree. Another criterion on choice of operating point is that the differential in ouput power between the driven and free modes be as large as possible. This gives the best measurement resolution. Usually this means a weak free oscillation is driven into a strong driven one. The signal averaging takes place over N gyrotron pulses ($N \cong 256$). A certain fraction of these pulses, ρ, will have a level I_1 corresponding to the free-running mode. The remaining fraction of the pulses, $(1- \rho)$, will have the level I_2 of the driven mode. A digitizing oscilloscope provides the average A:

$$A = \frac{1}{N}\left\{\sum_{i=1}^{\rho N}(I_1 + \Delta I_{1_i}) + \sum_{i=1}^{(1-\rho)N}(I_2 + \Delta I_{2_i})\right\} \qquad (10)$$

where random pulse-to-pulse fluctuations in oscillation amplitude, ΔI_i, are included. Equation (10) can be rewritten:

$$A = \sum_{i=1}^{\rho N}\frac{\Delta I_{1_i}}{N} + \sum_{i=1}^{(1-\rho)N}\frac{\Delta I_{2_i}}{N} + \rho I_1 + (1-\rho)I_2 \qquad (11)$$

The first two terms in equation (11) are assumed to vanish. Though the fluctuations ΔI_1 and ΔI_2 are random from pulse to pulse, their average cannot be neglected unless $\frac{\Delta I}{I} << 1$ and a large number of pulses are included in the average. Though the first condition holds in the experiment the second does not hold in the limits where there is very little control over the free mode or the mode is almost completely controlled. The experimental errors are expected to be correspondingly larger in these regions. The fraction of missed pulses (those not in the driven mode) is therefore:

$$\rho = \frac{A - I_2}{I_1 - I_2}$$

It is this fraction ρ which is the measure of the degree of coupling of the drive signal to the electron beam.

Fig. 16 shows the results for drive power injection using one and two probes. The three experiments shown involve measurement of missed pulses as a function of drive power. Drive power is injected three different ways and the results are

shown as a function of the power into the RHCP wave in each case. The first experiment is single probe drive. The power into the RHCP wave is determined from equation (5). The second experiment consists of driving two probes with equal amplitudes and 90° out of phase. This configuration generates a pure RHCP wave with a power level given by equation (9). The last experiment shown in the figure utilizes two probes with arbitrary input amplitudes and 90° out or phase. The power into one probe is held constant while that into the second is varied. Equation (8) is used in this case to determine the coupling to the RHCP wave.

The general result in all the experiments is that, as before, the degree of mode control decreases with decreasing drive power. It is clear from Fig. 16 that regardless of how the amplitude of the drive signal is varied, the degree of mode control only depends upon the drive power in the RHCP wave. From this, it can be inferred that the electromagnetic wave only couples to the gyrating electron beam, through electron cyclotron absorption, when the wave is RHCP.

A further test of this conjecture is provided by an experiment in which the drive power is constant but the phase between the two driven probes is varied. The drive power input to each probe is approximately equal. The results of this investigation are shown in Fig. 17. The fraction of missed pulses, ρ, varies approximately sinusiodally with the phase angle Θ. This is to be expected if the degree of mode control is simply proportional to the drive power input in a RHCP wave since the power into the two circularly polarized waves in this experiment is (from equation (7)):

$$\langle P \rangle = \frac{1}{2} P_{IN} \pm \sqrt{P_1 P_2} \sin \Theta \quad . \tag{12}$$

Fig. 16 shows, however, that the relationship between mode control and RHCP drive power is not quite linear. Of more importance is the location of the points of maximum and minumum mode control. The first minima of Fig. 17 occurs at ~ 130° (probe #4 leading probe #3 in Fig. 2(b)). When the 32° line length correction is taken into account the point of maximum mode control is found to be ~ 98°. This is

quite close to the 90° interprobe phase shift required to produce a pure RHCP wave, (see equation (13)). The first maxima occurs at a corrected phase shift of 302°, reasonable close to the 270° required for excitation of a pure LHCP wave.

In conclusion, given a fixed amount of drive power the most efficient means of coupling to the electron beam is at an interprobe phase shift such that a pure RHCP wave is launched into the cavity. Alternatively, given a fixed phase shift between probes the amplitudes should be adjusted so that as much drive power as possible is in the form of a RHCP wave.

Theory does not predict exactly zero coupling between the LHCP wave and the electron beam or perfect coupling for the RHCP wave when the TE_{11} field pattern and the annular electron beam geometry are taken into account. A more realistic prediction can be made by calculation of the beam-wave coupling coefficient as defined by Chu.[32] The interaction between the beam and the electromagnetic wave is really only dependent on the electric field strength tangential to the electron orbit. The beam power gain is proportional to the square of this electric field. Expanding the electric field of a circular TE_{mn} mode about an off-axis electron gyro-center yields:[33]

$$E_\phi = \frac{1}{2} k_{mn} C_{mn} J_{m-1}(k_{mn} R_o) \left[J_0(k_{mn} r_L) - J_2(k_{mn} r_L) \right] \cos(\omega t - \phi)$$

where C_{mn} is a constant defined in ref (33), R_o is the guiding center radius, k_{mn} is the transverse wavenumber, r_L is the electron Larmor radius, and ϕ is the azimuthal coordinate. Here only the first spacial harmonic is considered. A thin ring of electrons with guiding centers at a radius R_o is assumed. In the experiment the right-hand wave has eigenvalues m=1, n=1 and the coupling coefficient is:

$$K_{RH} = \left\{ J_0(k_{11} R_o) \left[J_0(k_{11} r_L) - J_2(k_{11} r_L) \right] \right\}^2 \qquad (13)$$

The coefficient of the left-hand wave (m=-1, n=1) is:

$$K_{LH} = \left\{ J_{-2}(k_{-11} R_o) \left[J_{-2}(k_{-11}\, r_L) - J_0(k_{-11}\, r_L) \right] \right\}^2 \qquad (14)$$

Using R_o = .9 cm and r_L = .23 cm, (consistent with a beam α of 1.0), the ratio of the coupling coefficients of equations (13) and (14) equals:

$$\frac{K_{RH}}{K_{LH}} = 55.2$$

As surmised, the theoretical coupling of the right-hand wave to the beam is much stronger than the left-hand. A rough experimental determination of this ratio can be made from the data of Figures 16 and 17. The missed pulse fraction can be eliminated from consideration by transforming ρ in Fig. 17 to power coupled into the right-hand wave as given in Fig. 16. The curve corresponding to pure right-hand wave excitation in Fig. 16 is used. This power is proportional to the actual power coupled to fields on the electron orbit (equation (13) gives the predicted coupling constant). Fig. 18 shows the new plot relating phase between the probes to power actually coupled into the fields on the electron orbit. The same sinusoidal shape as Fig. 17 is apparent here.

The power on orbit is produced from the separate contributions of the left- and right-hand circularly polarized waves, (as given by equation (12):

$$P_{orbit} \sim (P_{IN} + \sqrt{P_1 P_2} \sin \Theta)\, K_R + (P_{IN} - \sqrt{P_1 P_2} \sin \Theta)\, K_L \qquad (15)$$

where K_R and K_L are proportional to the coupling coefficients of the right- and left-hand polarized waves to the wave on the electron orbit. Varying the coefficients K_R and K_L to match the data in Fig. 18 results in the solid line for a coupling coefficient ratio $\left(\frac{K_R}{K_L}\right)$ of 55.2. The curve has been adjusted for the 10^o systematic error apparent

in Fig. 17. There is some difference in the predicted extrema in the sinusoid but the overlap with the experimental points is fairly good. One major uncertainty in this analysis is that the averaging method, upon which the measurement of the missed pulse fraction is based, suffers its largest uncertainty in the regions of very weak and very strong mode control. This means that the data points at the extrema in Fig. 18 are not very accurate. In addition, translating small or large missed pulse fractions into equivalent power via Fig. 16 is not precise. For example an uncertainty in the missed pulse fraction of 1 % at the maximum point in Fig. 17 causes uncertainties in the coupling ratio of a factor of two since Fig. 16 gives normalized powers anywhere between .5 and 1.5. It is found that variation of the coupling coefficient ratio by a factor of two in equation (15) still produces reasonable agreement with the experimental points in Fig. 18. Thus it seems that the measurement of the relative coupling strength of the right- and left-hand waves is in agreement with theory though the experimental uncertainties are factors of two.

V. Conclusion

Injection priming by an external signal is shown to be a powerful and flexible means of mode control in an overmoded gyrotron. The priming technique makes a much larger region of gyrotron parameter space accessible to pure mode operation. The technique is effective, to some degree, for all axial modes which otherwise would suffer mode skipping or stable parasitic oscillation. It is anticipated that this technique will also enable control of transverse modes as long as the filling factors of the different modes are similar.

A measurement is made of the relative coupling of the right- and left-hand circularly polarized waves to the electron beam. It is found, as predicted from theory, that the right-hand circularly polarized wave is the dominant electromagnetic wave involved in the electron cyclotron resonance mechanism. The experimental relative coupling strength agrees with the theoretical value to within experimental uncertainties.

VI. Acknowledgments

The help of W.M. Bollen in experimental setup and R.K. Parker in technical support is gratefully aknowledged. The authors also thank S. Swiadek and F. Wood for construction of the gyrotron tube.

References

1. K. Felch et al., in *Conference Digest of the Eleventh International Conference on Infrared and Millimeter Waves*, Pisa, Italy, 1986, p. 43.
2. K.E. Kreischer, S. Spira and R.J. Temkin, in *Conference Digest of the Eleventh International Conference on Infrared and Millimeter Waves*, Pisa, Italy, 1986, p. 229.
3. K.E. Kreischer, R.J. Temkin, H.R. Fetterman and W.J. Mulligan, IEEE Trans. Microwave Theory Tech. **MTT-32**, 481 (1984).
4. V.A. Flyagin, A.L. Gol'denberg, and G.S. Nusinovich in *Infrared and Millimeter Waves* vol. 11 (Academic Press, New York, 1984) p. 209-215.
5. G.S. Nusinovich, Izv. Vyssh. Ucheb. Zaved. Radiofiz. **18**, 1689 (1975).
6. A.K. Ganguly and K.R. Chu, Int. J. Electron. **51**, 503 (1981).
7. V.S. Ergakov and M.A. Moiseev, Radiophys. Quantum Electron. **18**, 89 (1975).
8. A.H. McCurdy et al., Phys. Rev. Lett. **57**, 2379 (1986).
9. I.I. Antakov, V.A. Gintsburg, E.V. Zasypkin and E.V. Sokolov, Elektronnaya Tekhnika, Elektronika SVCh, ser. 1, **8**, 20 (1975).
10. A.G. Luchinin and G.S. Nusinovich, Elektronnaya Tekhnika, Elektronika SVCh, ser. 1,**11**, 28 (1975).
11. D.B. McDermott and N.C. Luhmann, Jr., Bull. Am. Phys. Soc. **30**, 1509 (1985).
12. S.N. Vlasov, L.I. Zagryadskaya, and I.M. Orlova, Radiotekh. Electron. **21**, 1485 (1976).
13. A.V. Gaponov et al., Int. J. Electron. **51**, 277 (1981).

14. Y. Carmel et al., Phys. Rev. Lett. **50**, 112 (1983).

15. K.E. Kreischer and R.J. Temkin, Int. J. Infrared and Millimeter Waves **2**, 175 (1981).

16. D.A. Howe, NBS Tech. Note 679, March 1976.

17. K.E. Kreischer and R.J. Temkin, Int. J. Infrared and Millimeter Waves **1**, 195 (1980).

18. W.E. Lamb, Jr., Phys. Rev. A **134**, 1429 (1964).

19. M.A. Moiseev and G.S. Nusinovich, Radiophys. Quantum Electron. **17**, 1305 (1974).

20. I.G. Zarnitsyna and G.S. Nusinovich, Izv. VUZ, Radiofizika **18**, 303 (1975).

21. G.S. Nusinovich, Int. J. Electron. **51**, 457 (1981).

22. A.H. McCurdy, C.M. Armstrong and W.M. Bollen, NRL Report 9038 (1987).

23. A.H. McCurdy and C.M. Armstrong, submitted to IEEE Trans. MTT.

24. J. Lachambre, P. Lavigne, G. Otis, and M. Noël, IEEE J. Quantum Electron. **QE-12**, 756 (1976).

25. E.E. David, Jr., Proc. IRE **40**, 669 (1952).

26. K. Felch, private communication; K. Felch, et al., Bull. Am. Phys. Soc. **31**, 1484 (1986).

27. V.S. Bazhanov, V.S. Ergakov, and M.A. Moiseev, Radiophys. Quant. Electron. **20**, 90 (1977).

28. R.S. Symons and H.R. Jory, in *Advances in Electronic and Electron Physics*, L.Marton and C. Marton, eds. (Academic Press, New York, 1981), vol 55, p. 24.

29. A.V. Gaponov, Izv. VUZ, Radiofizika **4**, no. 3, 547 (1961).

30. A.V. Gaponov and V.K. Yulpatov, Radioteknika i elektronika **12**, 627 (1967).

31. F.E. Ehlers, in *Microwave Transmission Circuits*, G. L. Ragan, ed. (McGraw-Hill, New York, 1948) p. 369.

32. K.R. Chu, Phys. Fluids **21**, 2354 (1978).

33. A.W. Fliflet, M.E. Read, K.R. Chu, and R. Seeley, Int. J. Electron. **53**, 505 (1982).

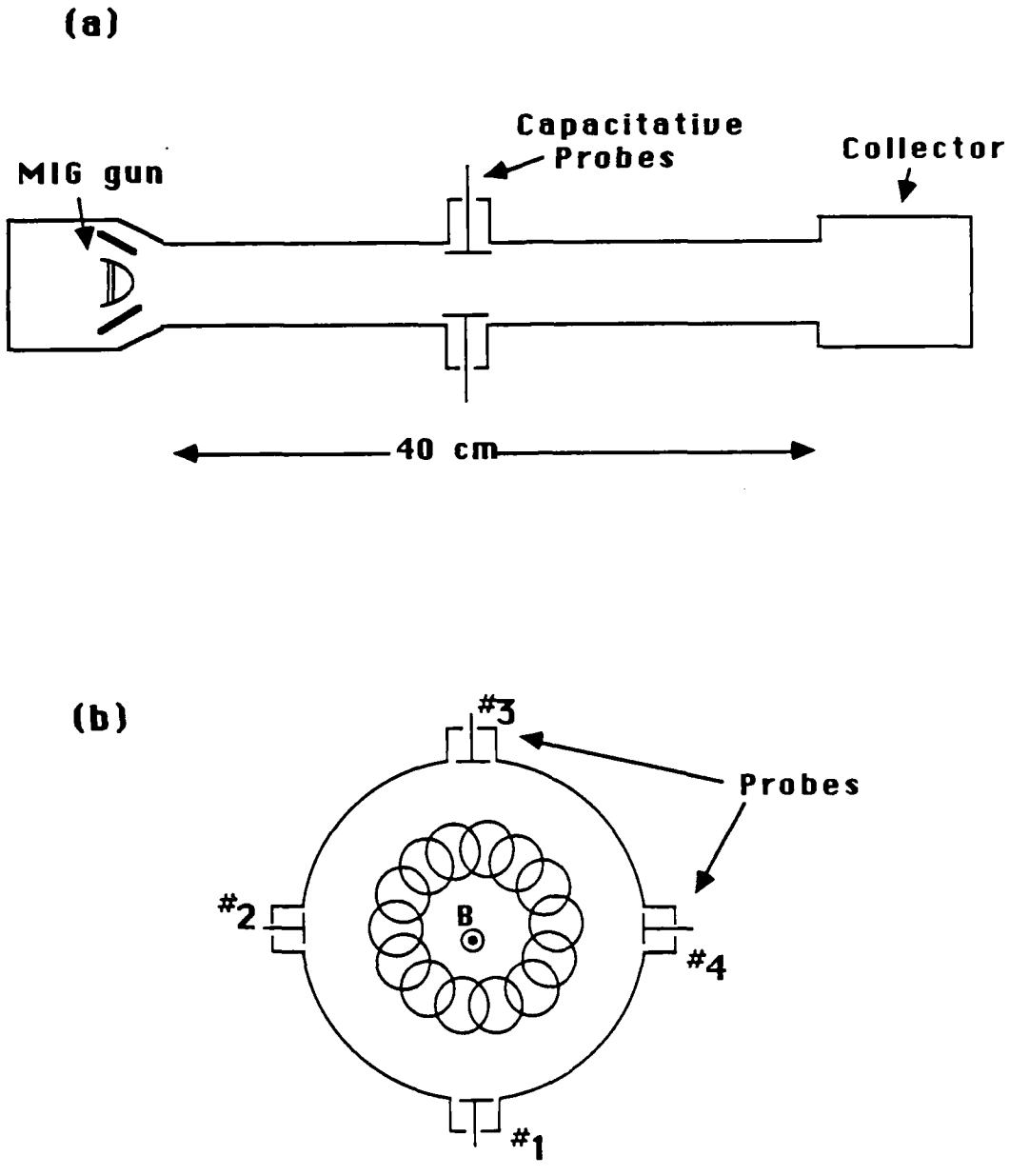

Fig. 1 Configuration of (a) the gyrotron oscillator and (b) probe geometry.

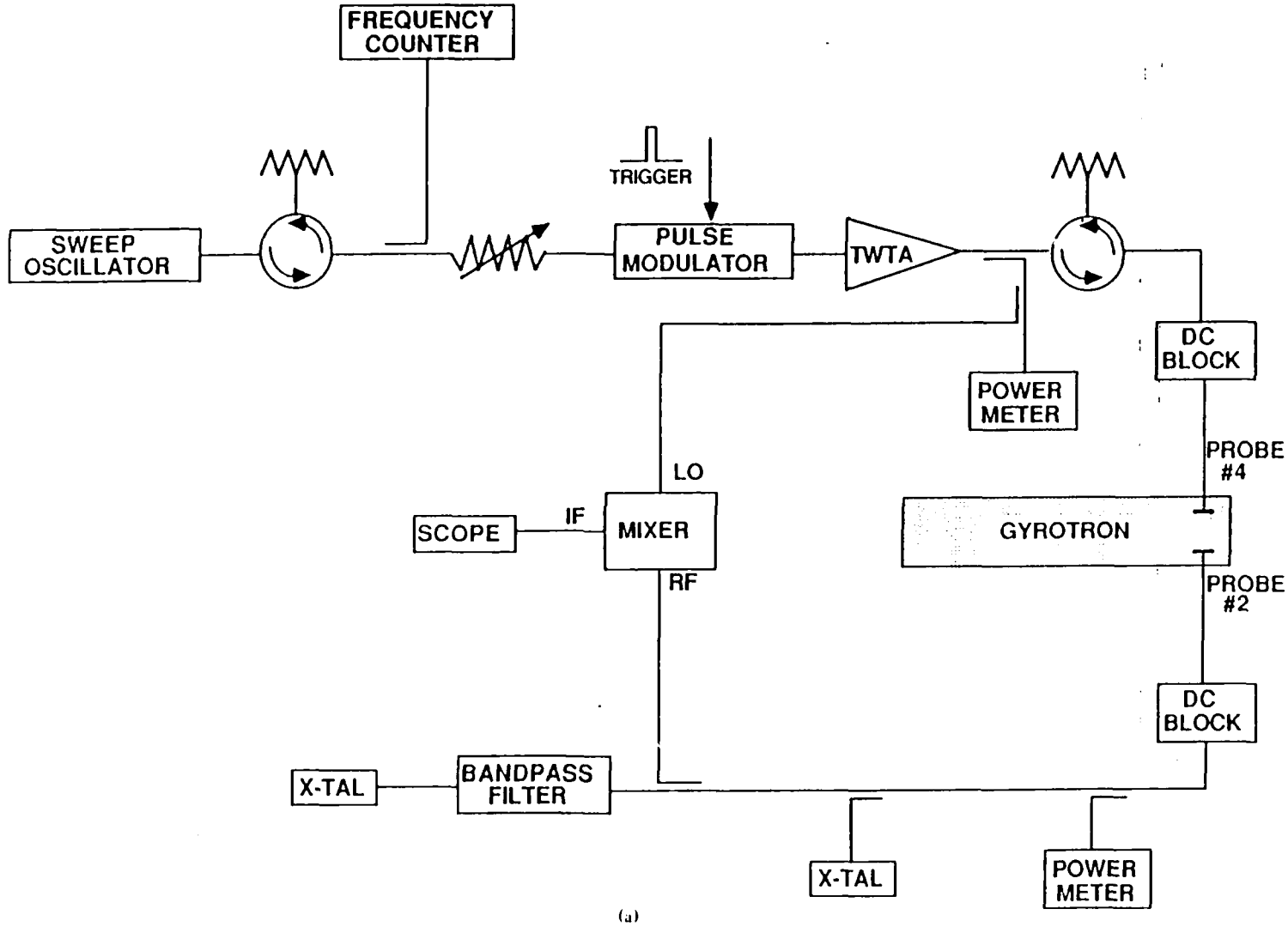

Fig. 2 Schematic of the (a) single probe (probe #4) injection and (b) two probe injection (probes #3 and #4) experiments. Gyrotron output is through probe #2.

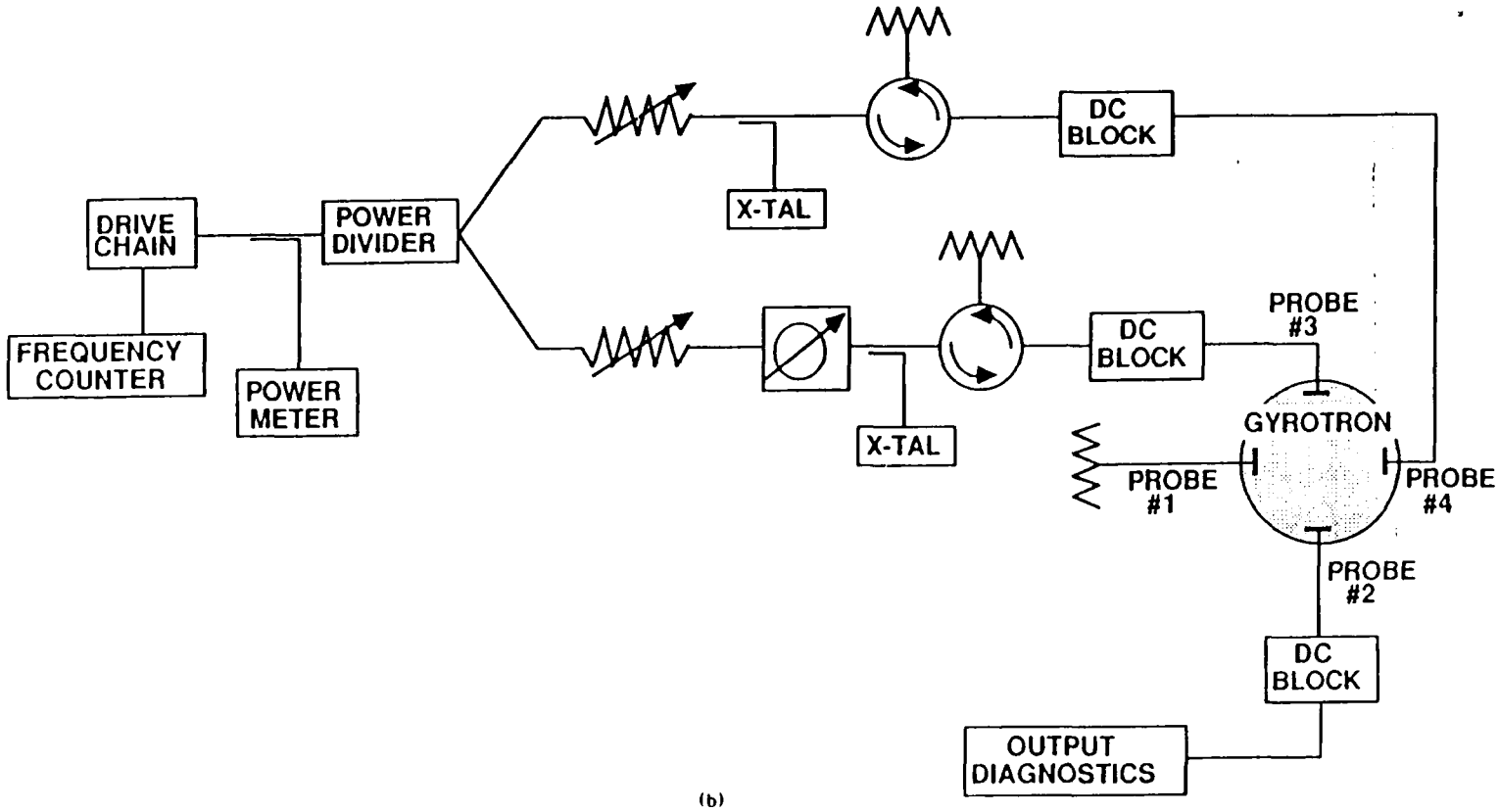

Fig. 2 (Continued) Schematic of the (a) single probe (probe #4) injection and (b) two probe injection (probes #3 and #4) experiments. Gyrotron output is through probe #2.

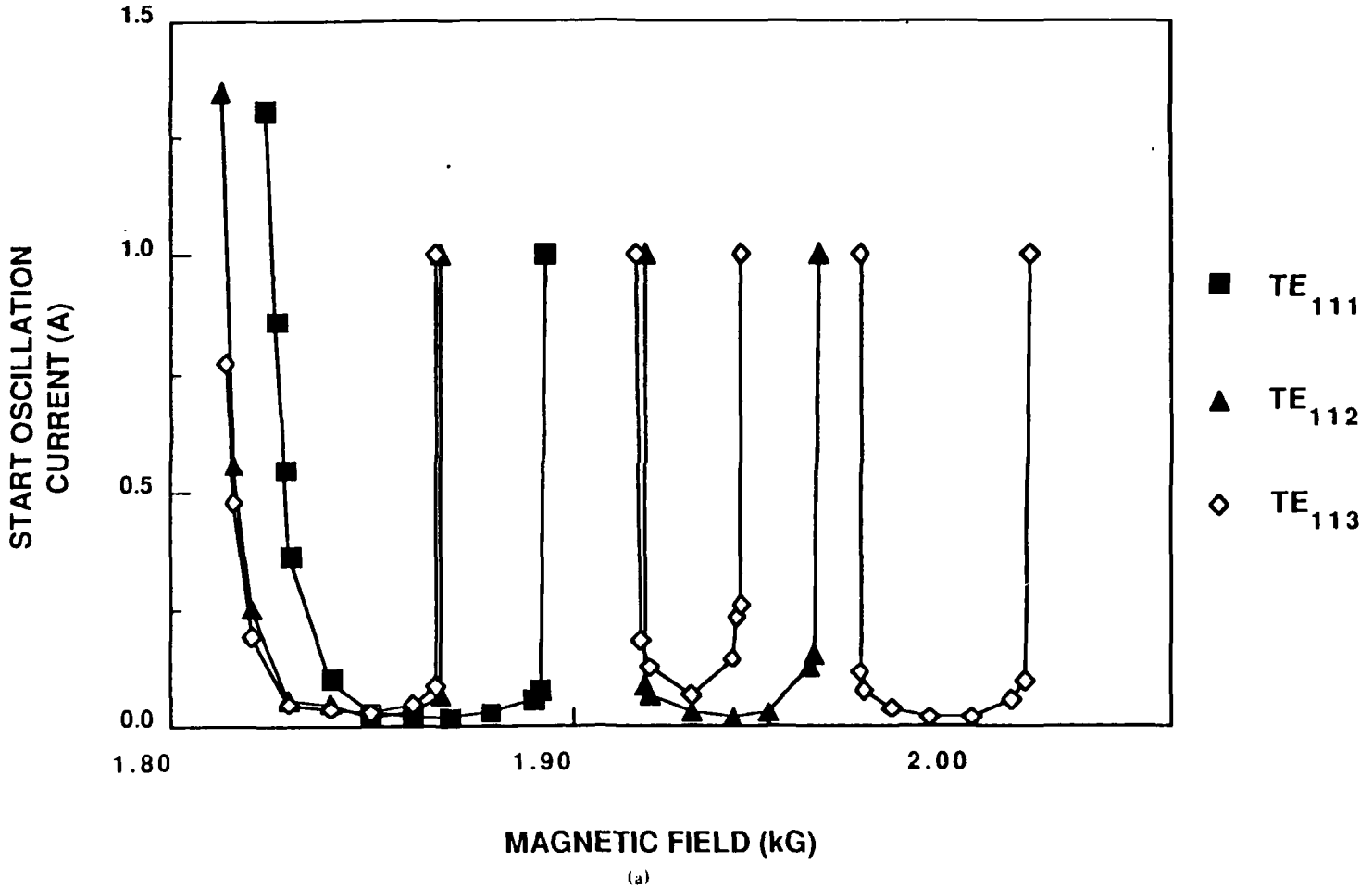

(a)

Fig. 3 Predictions of single mode linear theory. (a) start oscillation currents and (b) frequency of oscillation for different modes.

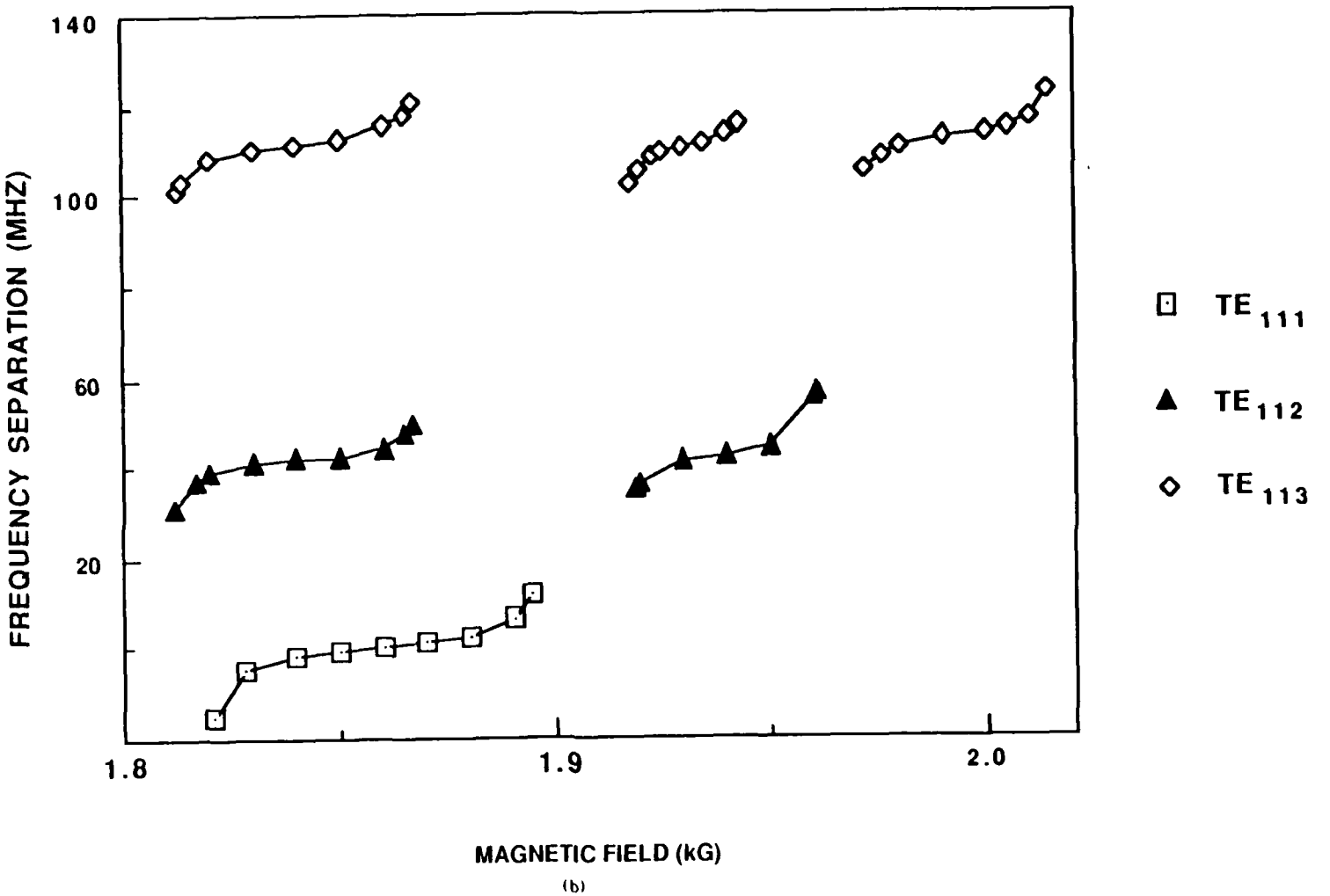

(b)

Fig. 3 (Continued) Predictions of single mode linear theory. (a) start oscillation currents and (b) frequency of oscillation for different modes.

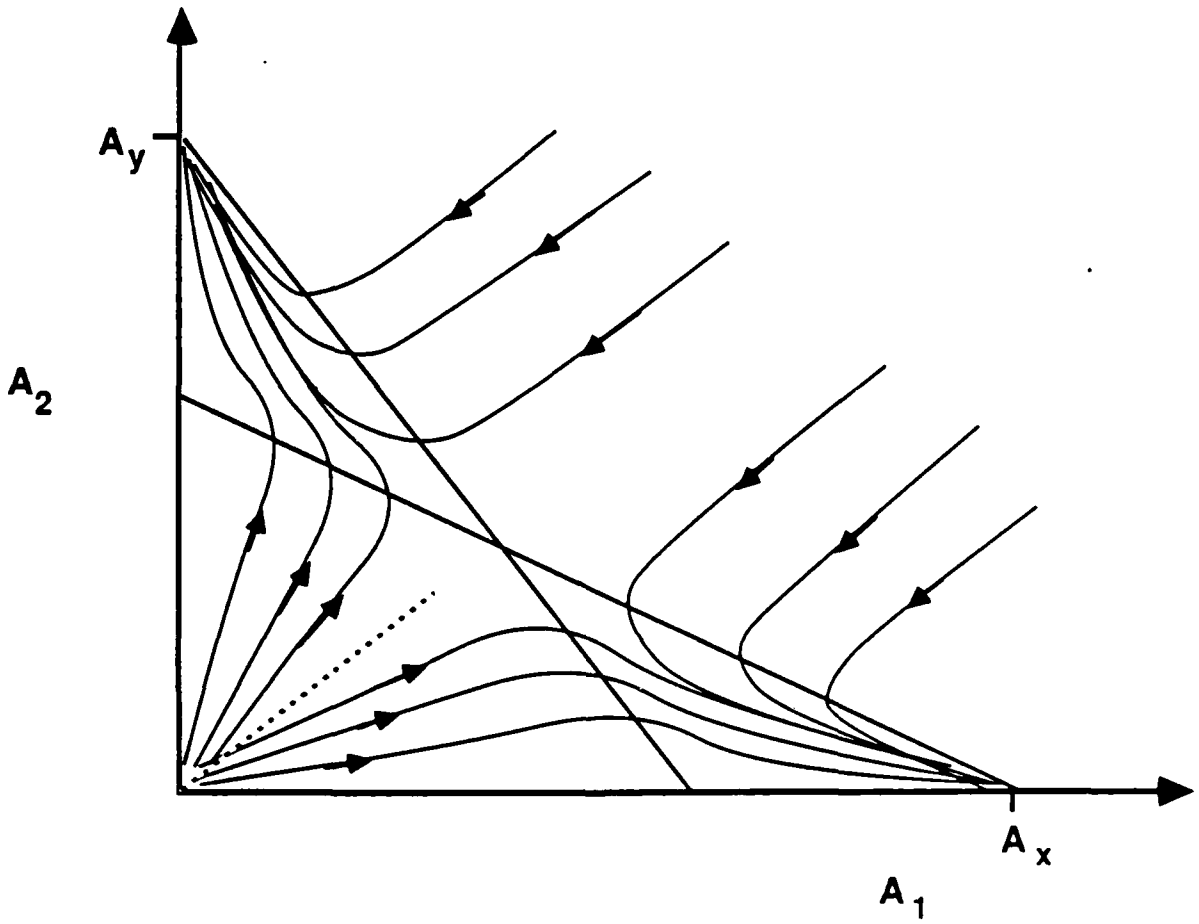

Fig. 4 Typical evolution of oscillation amplitudes in two-mode system with strong coupling. The steady state equilibrium amplitudes are (A_1=0, A_2=A_y) and (A_1=A_x, A_2=0).

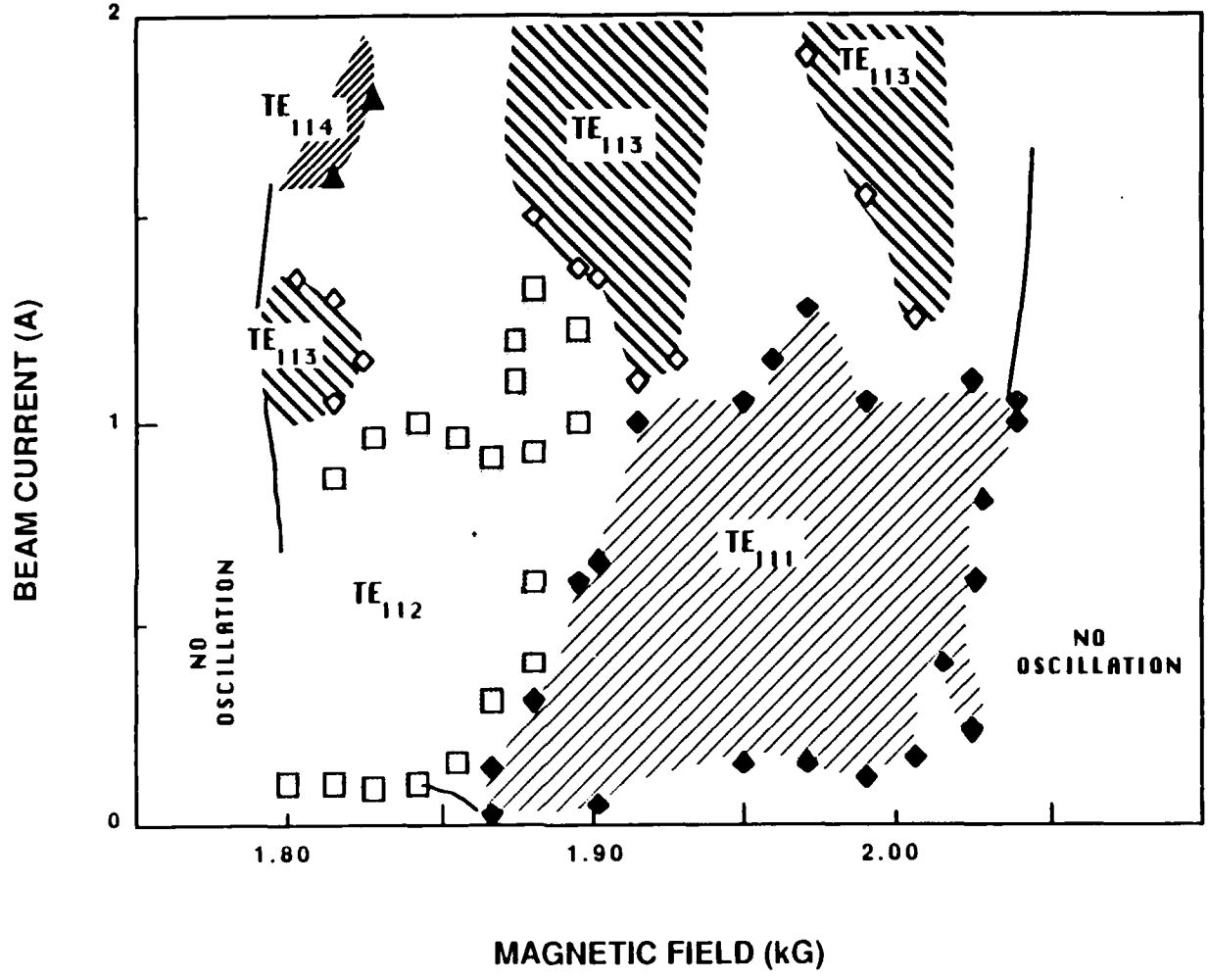

Fig. 5 Regions of pure mode excitation in the undriven gyrotron I-B parameter space.

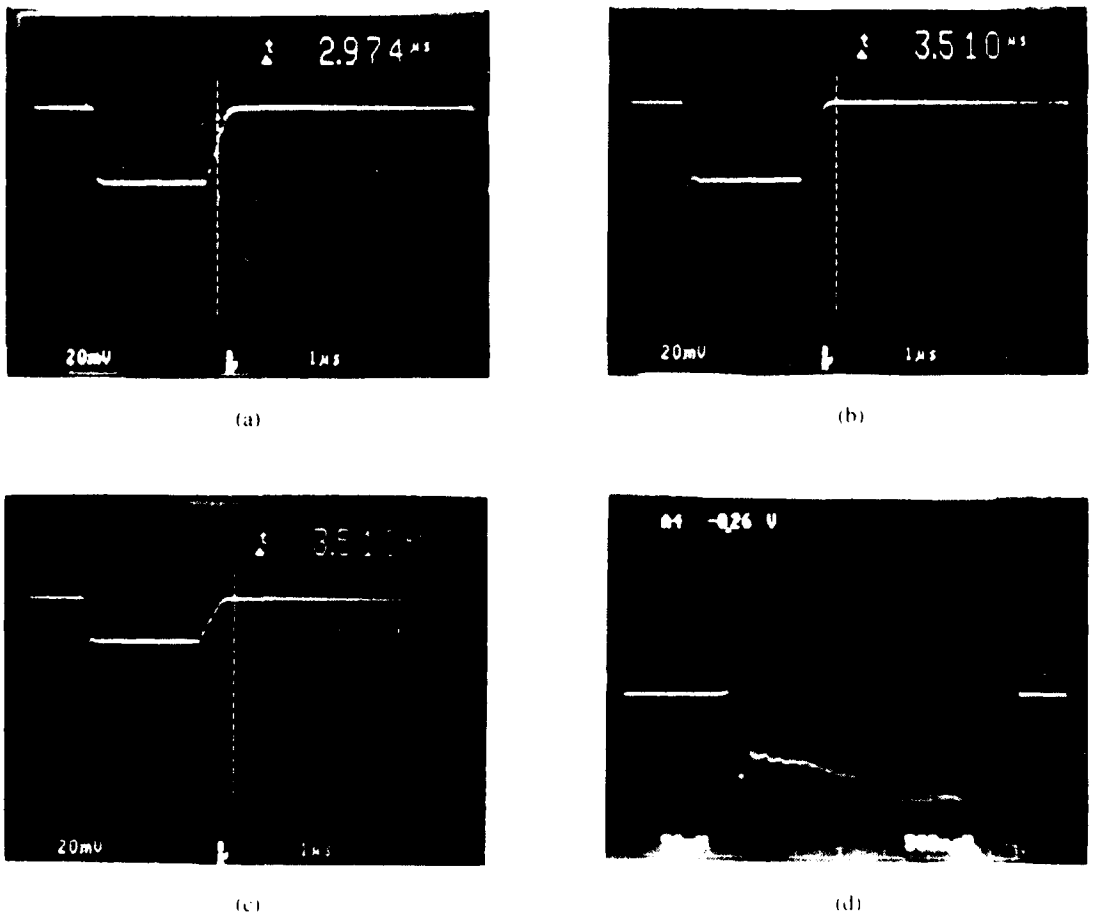

Fig. 6 Stabilization of mode skipping. (a) free, unfiltered gyrotron output skipping between TE_{111} (upper trace) and TE_{112} modes. Gyrotron output with (b) driving frequency at 5.141 GHz, (TE_{112} frequency), yielding pure TE_{112} mode and (c) drive at 5.093 GHz, (TE_{111} frequency), resulting in pure TE_{111} output. Drive power is .7 W. (d) relative phase between drive and gyrotron oscillation.

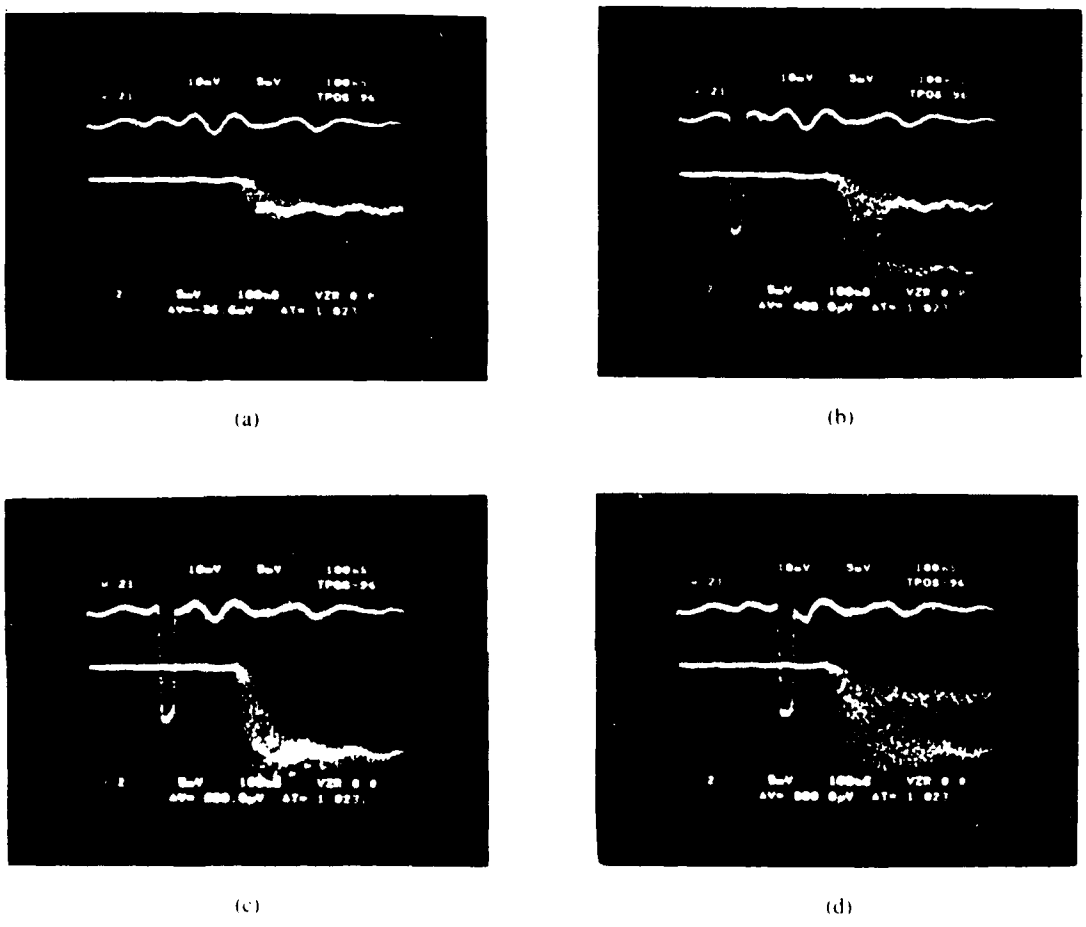

(a) (b) (c) (d)

Fig. 7 Temporal dependence of mode priming. Drive signal is upper trace while gyrotron output is lower. (a) free oscillation, Skipping between TE_{111} and TE_{113} modes (TE_{113} upper level). (b) ~50 ns drive pulse, (at frequency of TE_{111}), applied too early in oscillation buildup. (c) drive pulse at correct instant to prime pure TE_{111} mode. (d) drive pulse too late.

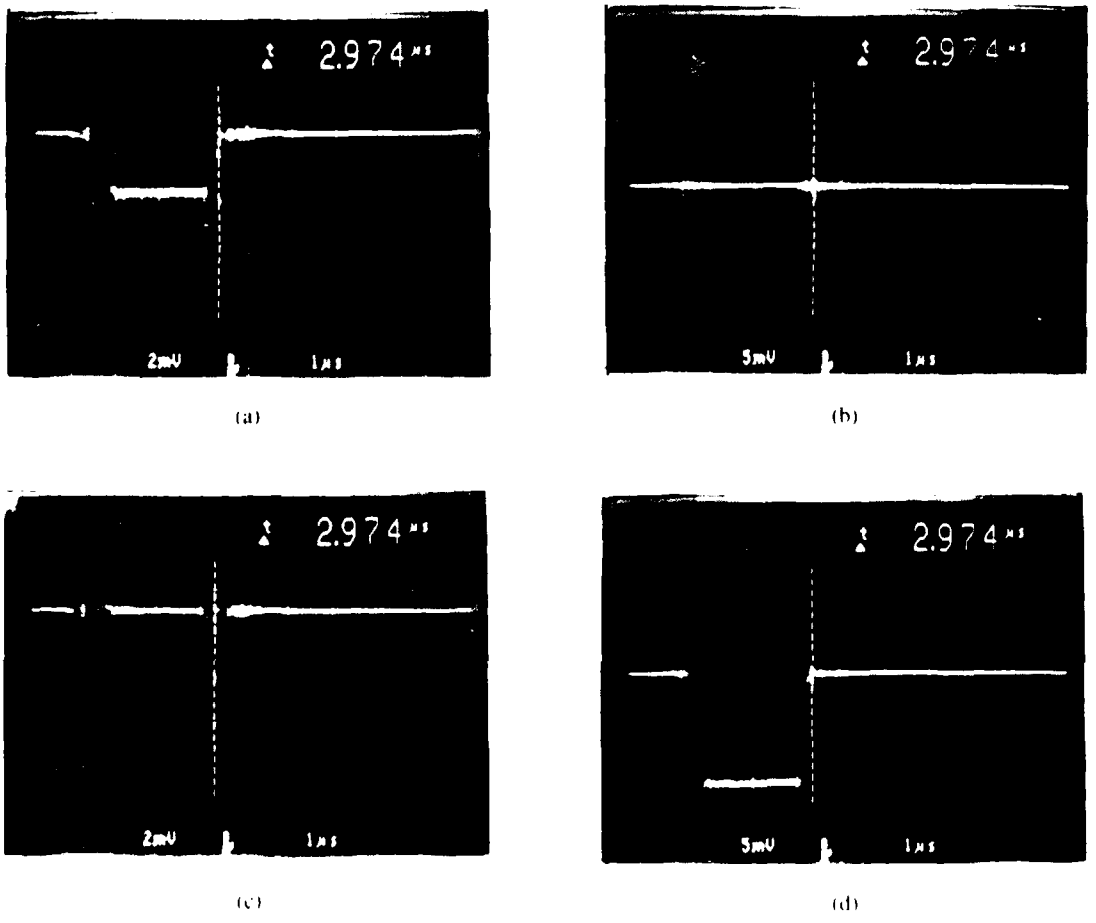

Fig. 8 Switch from steady TE_{113} mode to TE_{112} mode by priming signal at frequency of TE_{112}. (a) filtered free output shows TE_{113} oscillation at 5.251 GHz and (b) no oscillation in TE_{112} mode at 5.186 GHz. When drive signal is present (c) the TE_{113} dissappears and (d) a pure oscillation exists in the TE_{112} mode.

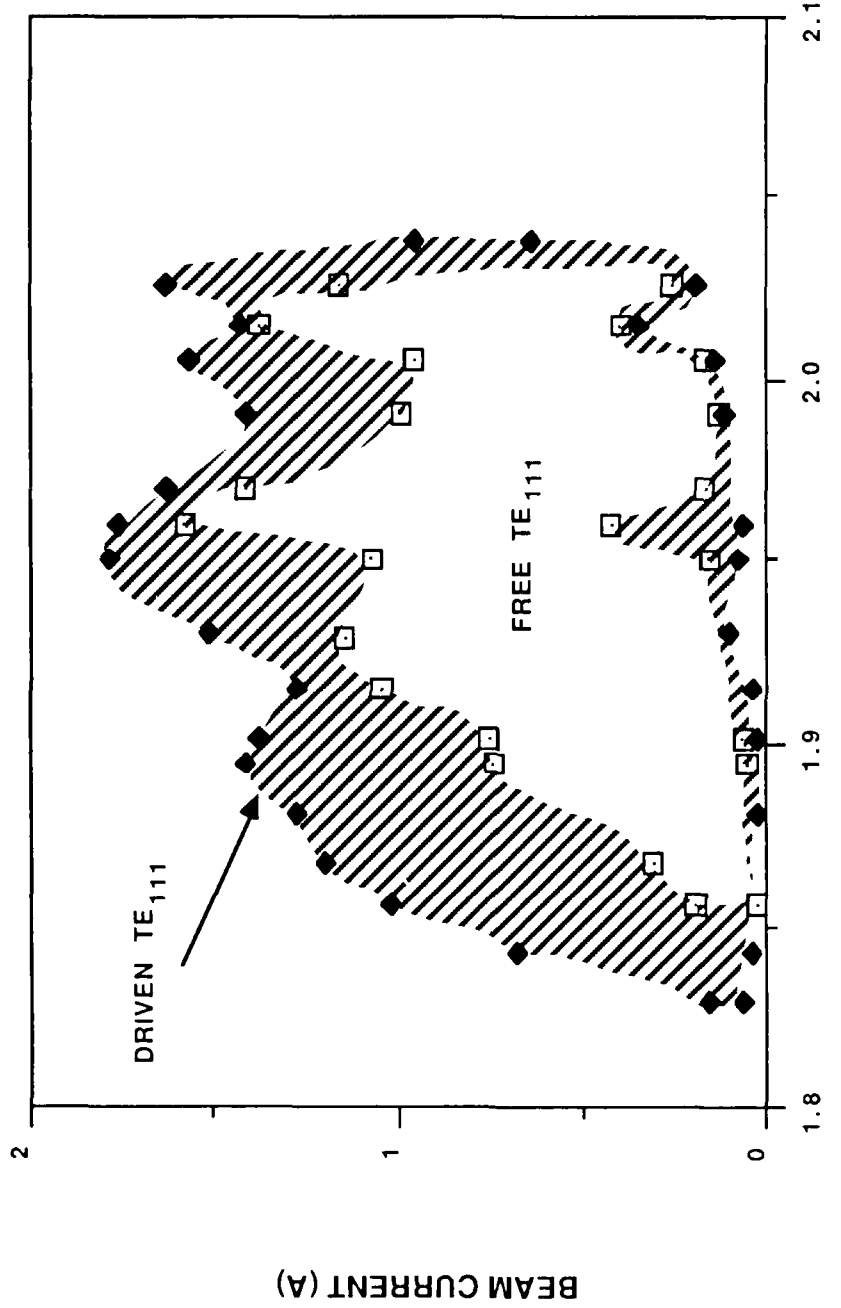

Fig. 9 Expansion of region of pure TE_{111} mode oscillation due to a 20 W driving signal.

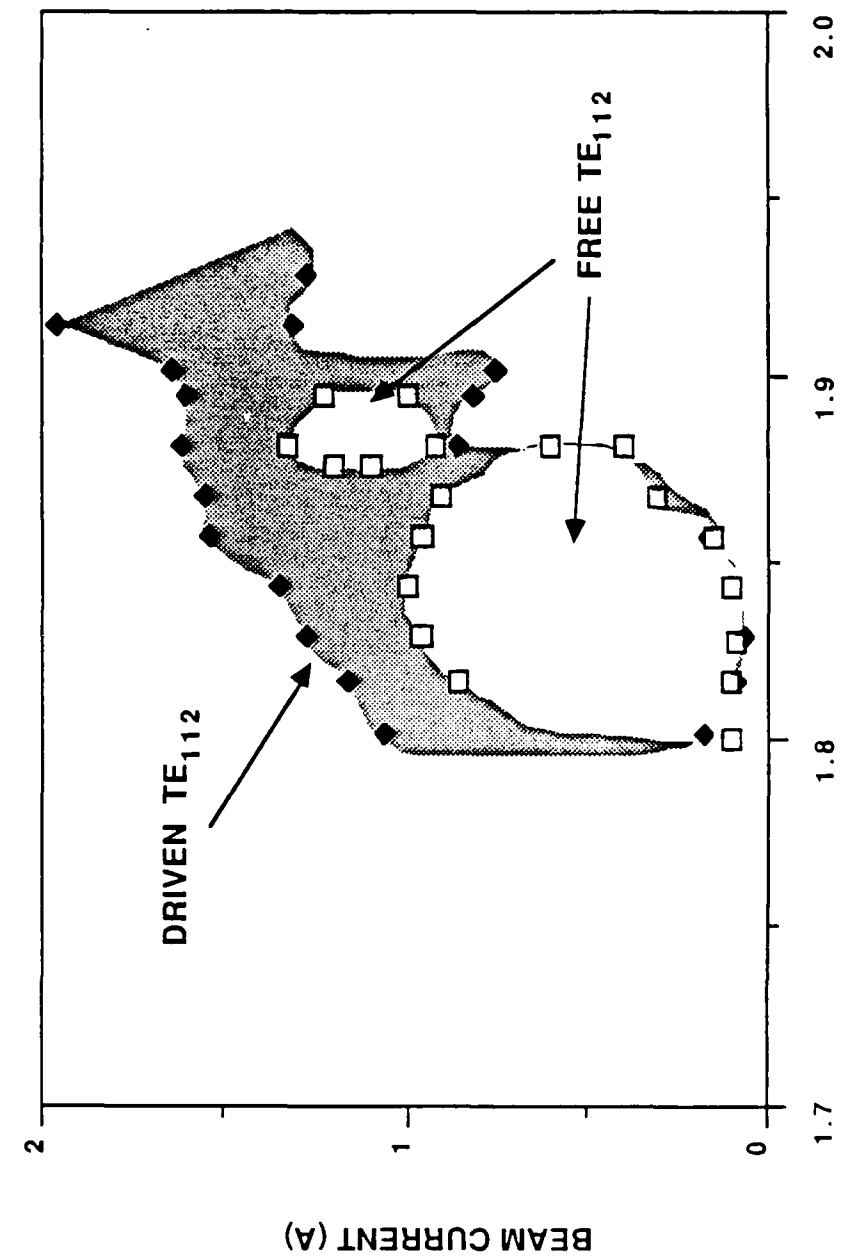

Fig 10 Expansion of region of pure TE_{112} mode oscillation.

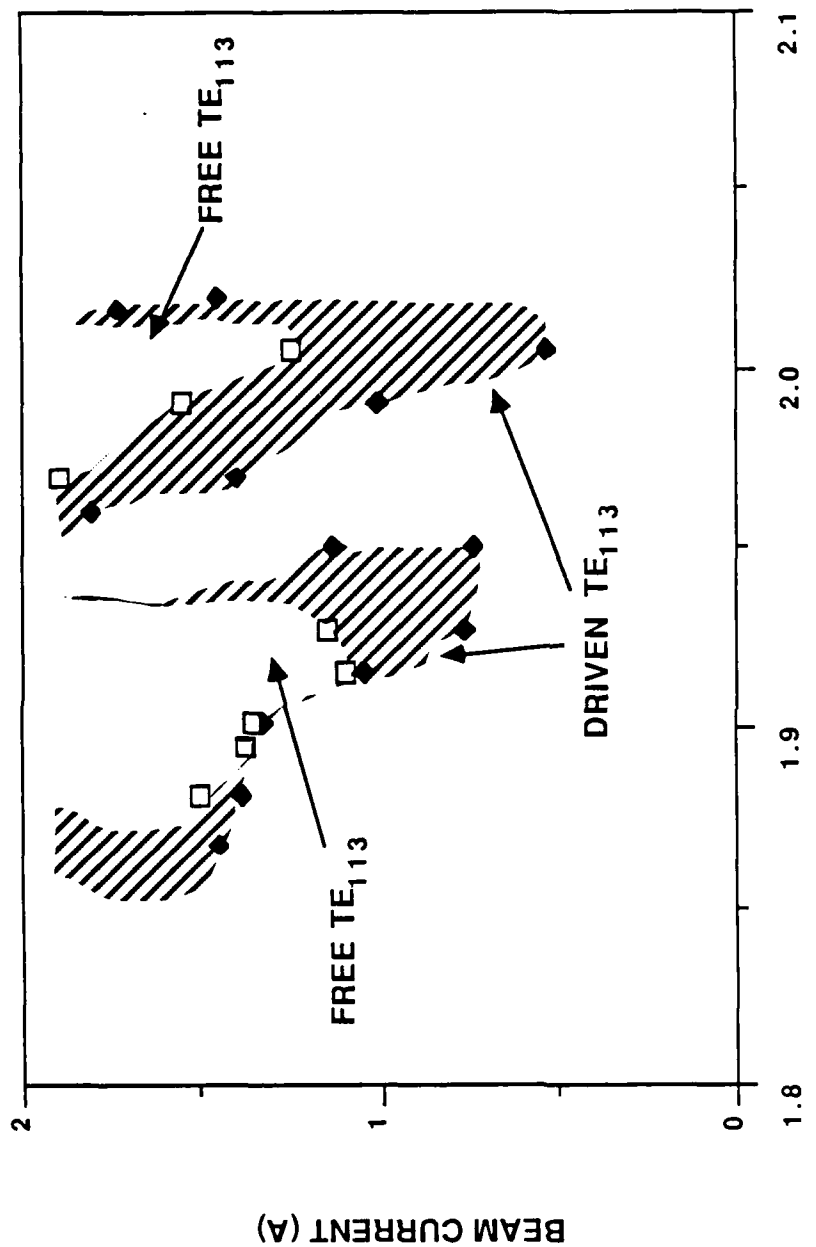

Fig. 11 Expansion of region of pure TE_{113} mode oscillation.

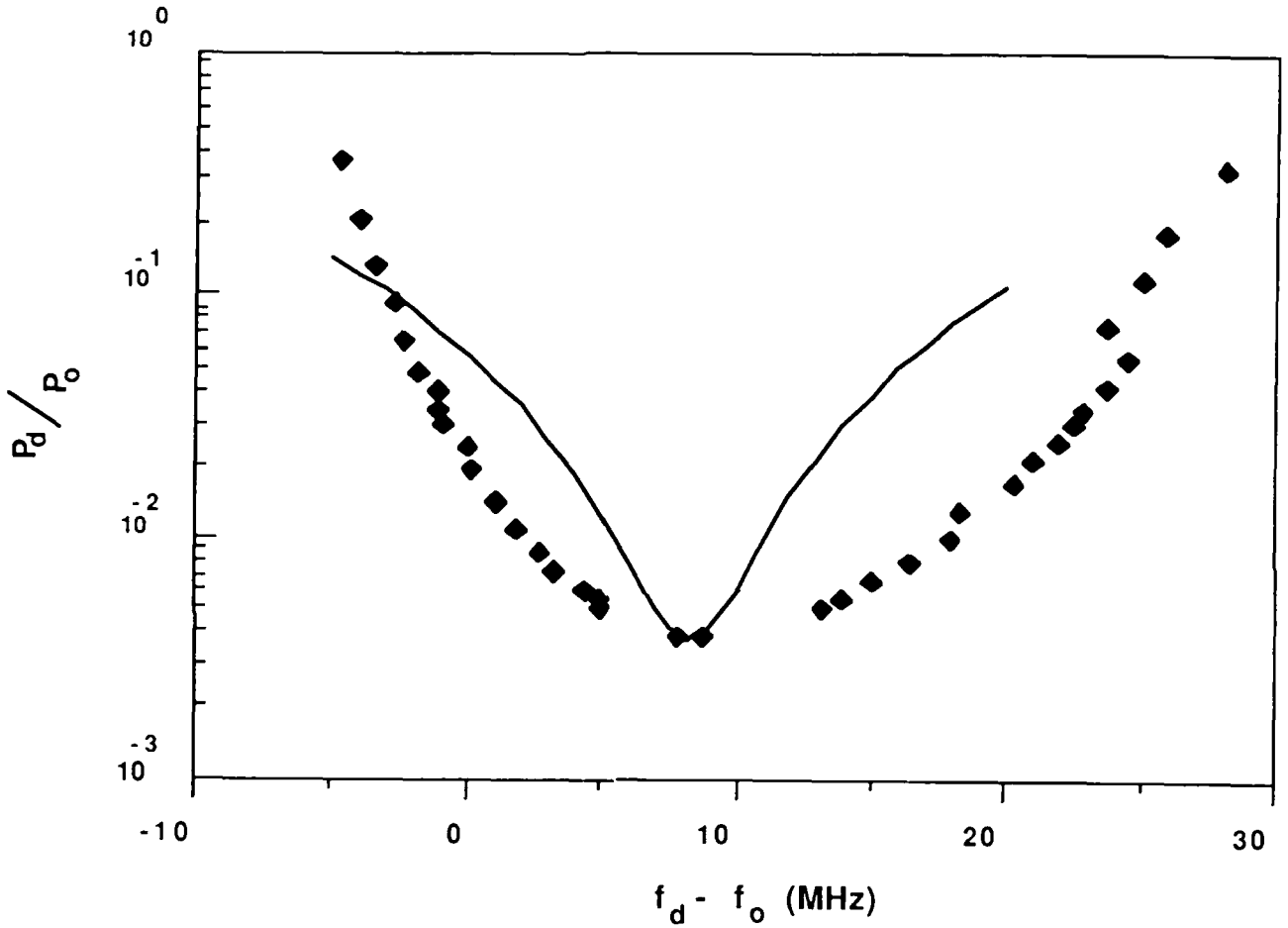

Fig. 12 Minimum drive power-to-oscillator power ratio required to prime pure TE_{111} mode from pure TE_{112} as a function of frequency separation between drive signal and TE_{111} oscillation. The solid curve shows the change in power coupled into the cavity due to finite cavity bandwidth.

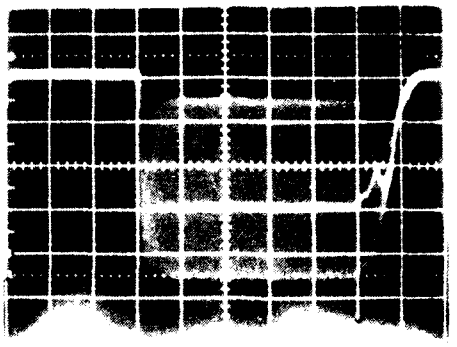

(a)

(b)

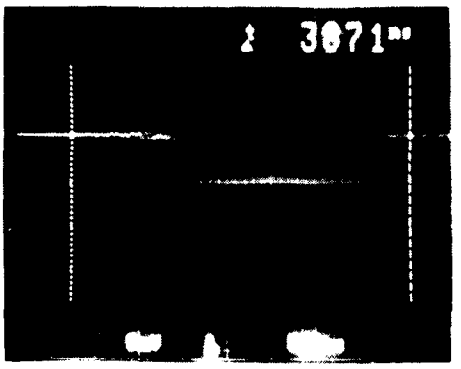

(c)

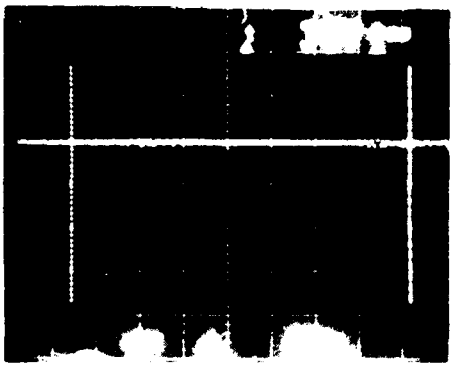

(d)

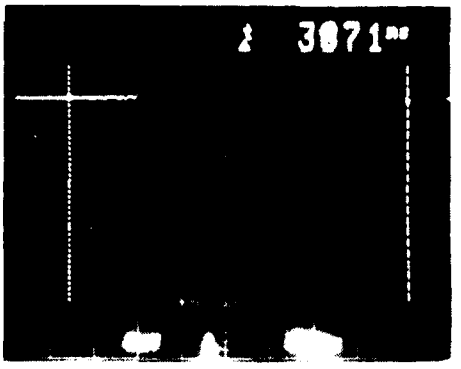

(e)

Fig. 13 Stabilization of bistable system. (a) free oscillation contains TE_{111} and TE_{112} simultaneously. Filtered output show (b) fast growing TE_{112} at 5.156 GHz and (c) slow growing TE_{111} at 5.099 GHz. Driving signal at 5.099 GHz (d) eliminates TE_{112} (bandpass filter at 5.156 GHz) and (e) enhances TE_{111} (filter at 5.099 GHz).

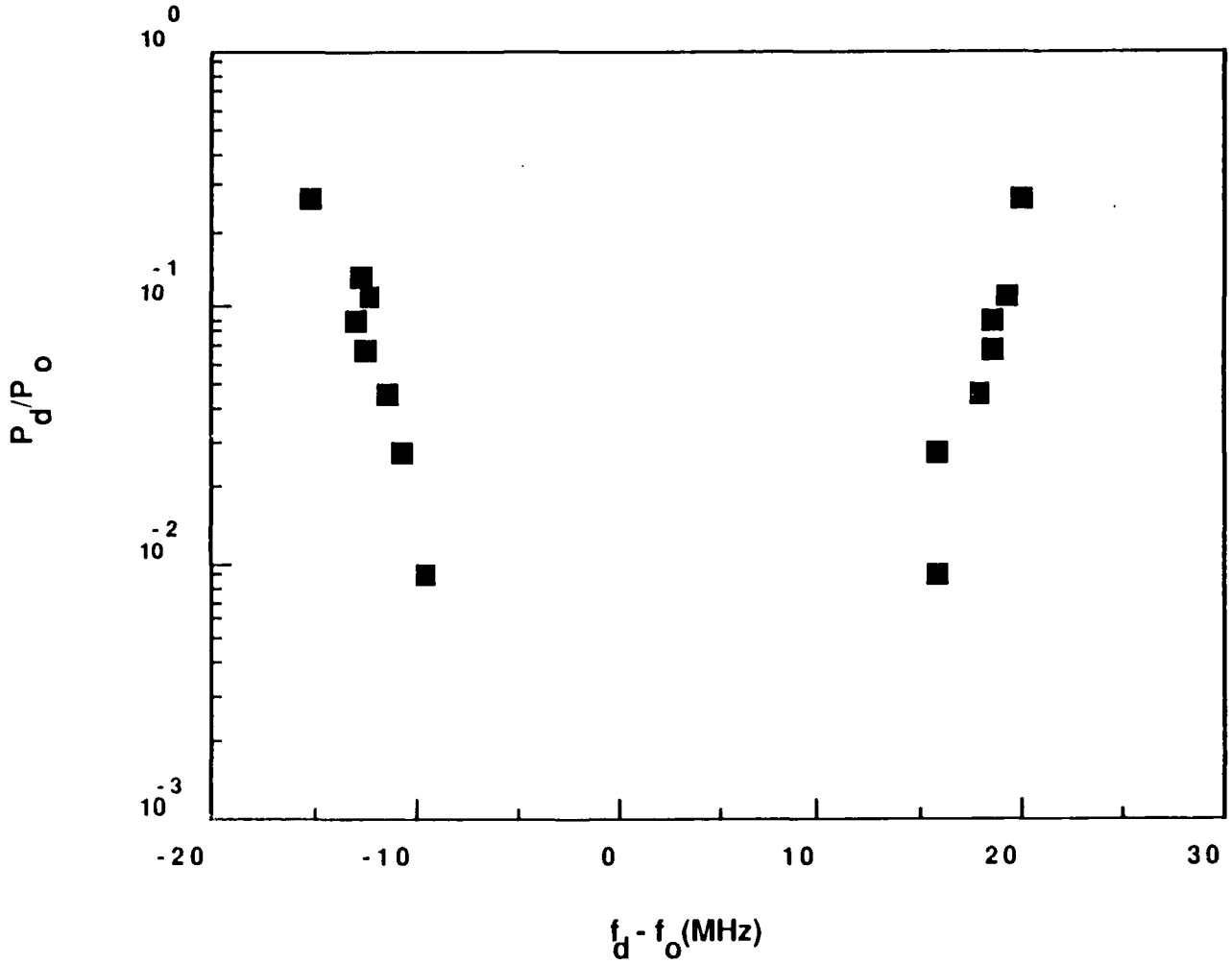

Fig. 14 Minimum drive-to-oscillator power ratio for mode priming second harmonic gyrotron operation. TE_{214} is primed from region of mode skipping.

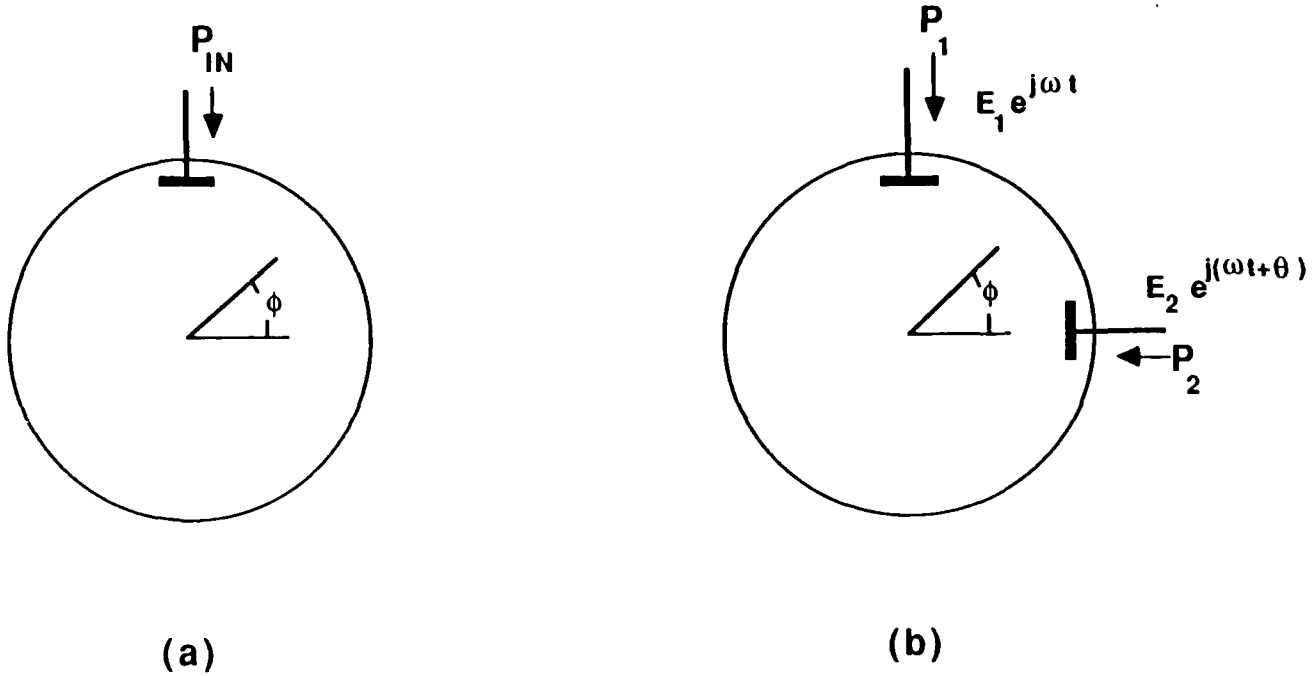

Fig. 15 Geometry for (a) one probe and (b) two probe excitation.

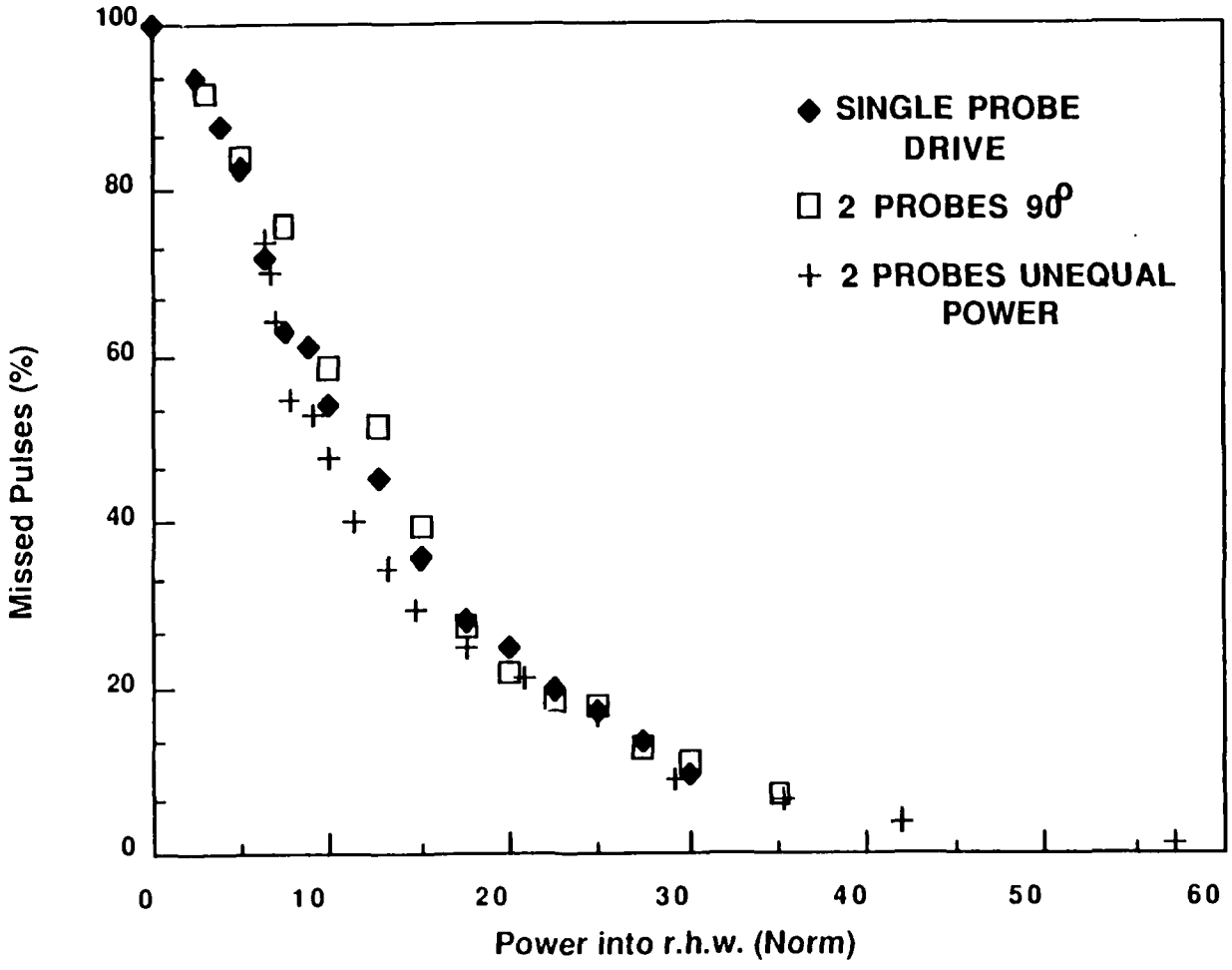

Fig. 16 Mode control as a function of normalized power into the right-hand circularly polarized electromagnetic wave. The three experiments shown invlove driving one probe, two probes with equal power and 90^0 phase lead on probe #2, and two probes at 90^0 with unequal power.

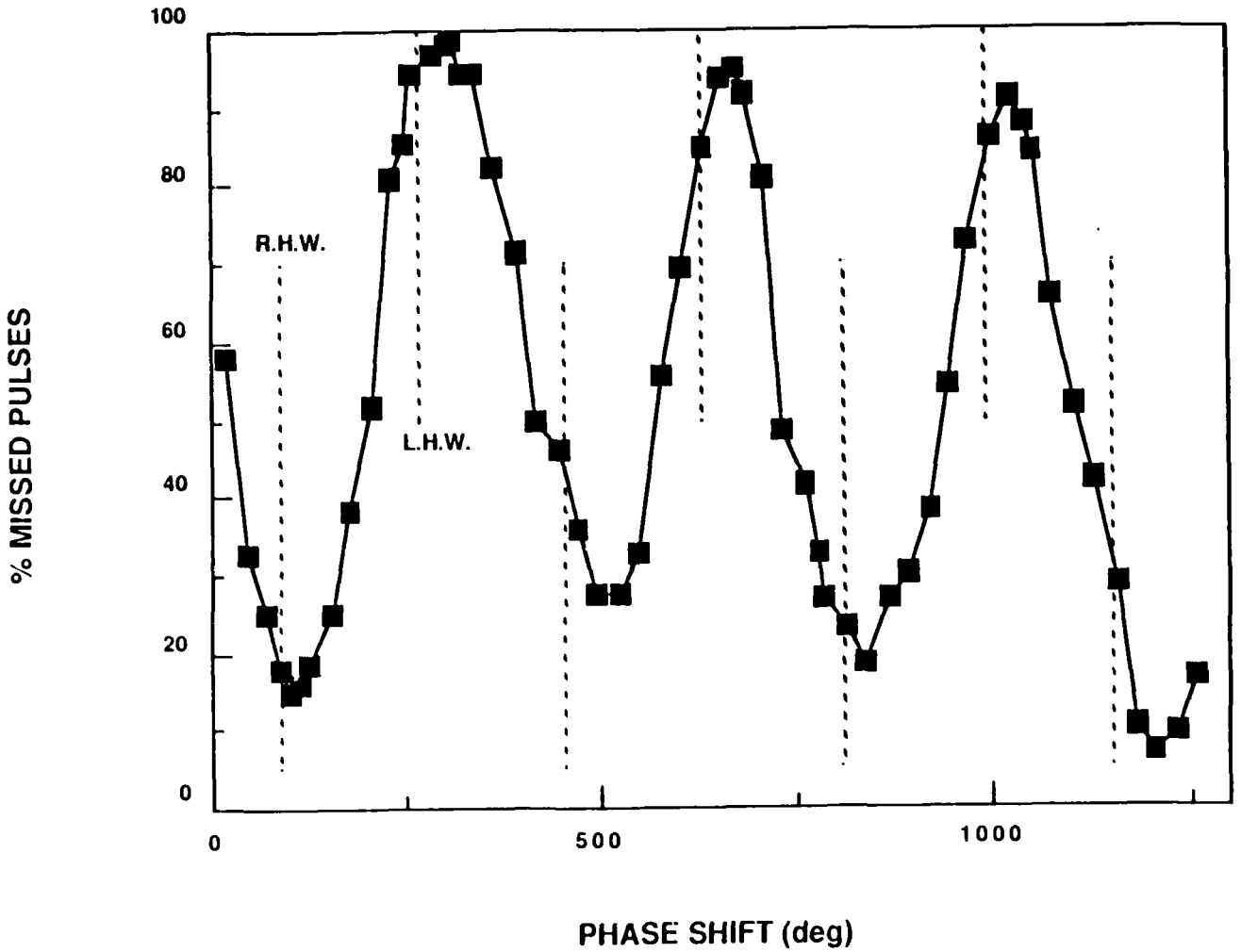

Fig. 17 Mode control as a function of phase shift between probes. Locations of nearly pure left- and right-hand waves are designated.

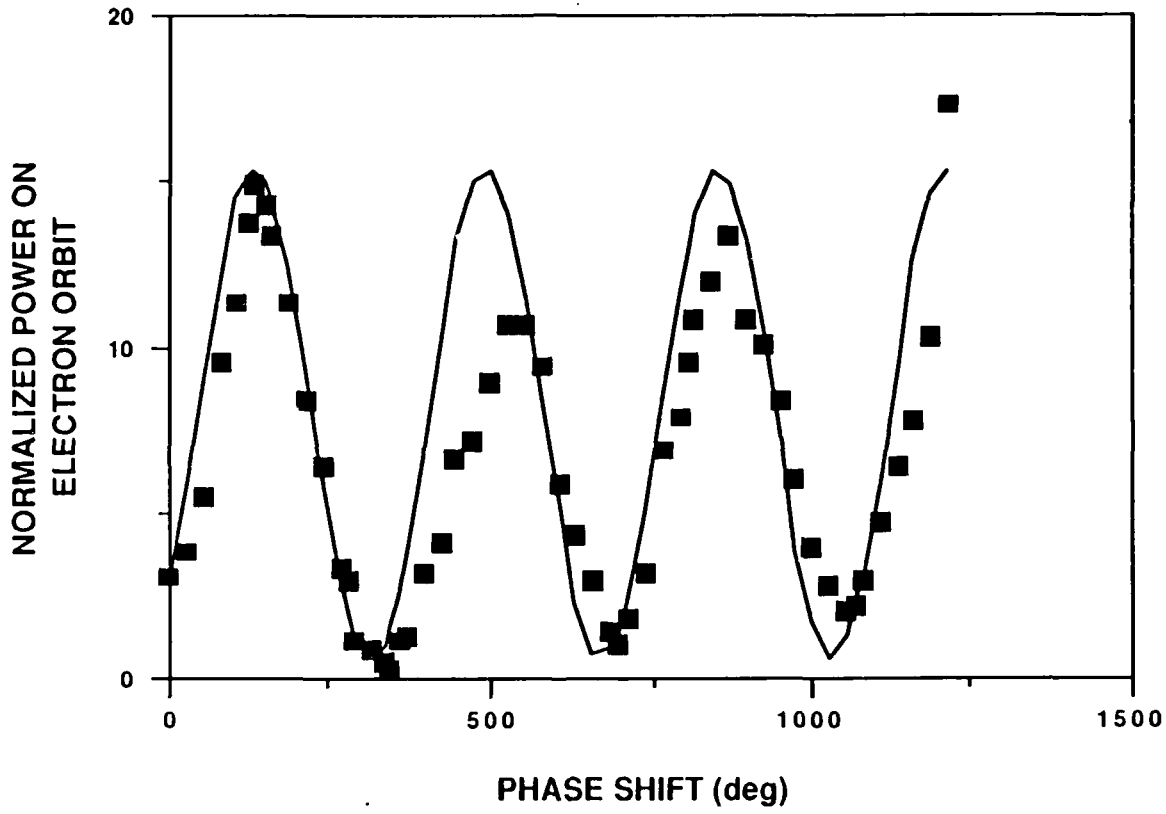

Fig. 18 Effective power on the electron orbit as a function of relative phase between probes. Solid line shows the theoretical prediction for a ratio between right- and left-hand coupling coefficients of 55.2.

END

DATE

FILMED

MARCH

1988

DTIC